M. BATTI

ATILIM UNIVERSITY 2020

CLOSED-LOOP DYNAMICS OF A CLASS OF HYBRID (MULTI-MODAL) FLYING ROBOTS

THE GRADUATE SCHOOL OF NATURAL AND APPLIED SCIENCES
OF
ATILIM UNIVERSITY

MOHAMED ISMAIL BATTI

IN PARTIAL FULFILLMENT OF THE REQUIREMENTS
FOR THEDEGREE OFDOCTOR OF PHILOSOPHY IN
MODELING AND DESIGN OF ENGINEERING SYSTEMS (MODES)
PhD PROGRAM

AUGUST 2020

CLOSED-LOOP DYNAMICS OF A CLASS OF HYBRID (MULTI-MODAL) FLYING ROBOTS

A THESIS SUBMITTED TO
THE GRADUATE SCHOOL OF NATURAL AND APPLIED SCIENCES
OF
ATILIM UNIVERSITY

BY

MOHAMED ISMAIL BATTI

IN PARTIAL FULFILLMENT OF THE REQUIREMENTS
FOR
THE DEGREE OF DOCTOR OF PHILOSOPHY
IN
THE DEPARTMENT OF MODELING AND DESIGN OF ENGINEERING SYSTEMS (MAIN FIELD OF STUDY: MECHATRONICS ENGINEERING)

AUGUST 2020

Approval of the Graduate School of Natural and Applied Sciences, Atılım University.

Prof. Dr. Ali Kara
Director

I certify that this thesis satisfies all the requirements as a thesis for the degree of **Doctor of Philosophy in Modeling and Design of Engineering Systems Department, Atılım University.**

Assoc. Prof. Dr. Ender KESKİNKILIÇ
Head of Department

This is to certify that we have read the thesis CLOSED-LOOP DYNAMICS OF A CLASS OF HYBRID (MULTI-MODAL) FLYING ROBOTS submitted by **Mohamed Batti** and that in our opinion it is fully adequate, in scope and quality, as a thesis for the degree of Doctor of Philosophy.

Prof. Dr. Hüseyin Nafiz Alemdaroğlu
Co-Supervisor

Asst. Prof. Dr. Kutluk Bilge Arıkan
Supervisor

Examining Committee Members:

Asst. Prof. Dr. Hakan Tora
Civil Aviation Aircraft Electrical and Electronics

Asst. Prof. Dr. Kutluk Bilge Arıkan
Mechanical Eng. Dept. , TED University

Asst. Prof. Dr. Mehmet Efe Özbek
Mechhanice Eng. Dept. , Atılım University

Asst. Prof. Dr. Ali EmreTurgut
Mechnical Eng. Dept. , METU

Asst. Prof. Dr. Selçuk Himmetoğlu
Mechanical Eng. Dept. , Hacettepe University

Date: 09. 08. 2020

I hereby declare that all information in this document has been obtained and presented in accordance with academic rules and ethical conduct. I also declare that, as required by these rules and conduct, I have fully cited and referenced all material and results that are not original to this work.

Name, Last Name: Mohamed Batti

Signature:

ABSTRACT

CLOSED-LOOP DYNAMICS OF A CLASS OF HYBRID (MULTI-MODAL) FLYING ROBOTS

Batti, Mohamed Ismail

PhD., Department of Modeling and Design of Engineering Systems

Supervisor: Asst. Prof. Dr. Kutluk Bilge Arıkan

Co-Supervisor: Prof. Dr. Hüseyin Nafiz Alemdaroğlu

August 2020, 55 pages

In this study, a class of hybrid flying robots is proposed in terms of the basic and advanced systems. Nonlinear and linearized mathematical models are derived for both of the systems in two-dimensional space. Linear quadratic regulator-based control systems are designed for the hovering and navigation scenarios. In addition, external forces are applied during the vertical takeoff, forward flight, and the land down. The differences between the linear and nonlinear responses are evaluated in addition to the differences between behaviors of the basic and advanced systems. It is shown that the admittance controller improves the stability of the basic system as the compelling external forces are applied. It is shown that both of the systems are suitable to be used as ground-air hybrid robotic platforms and aerial manipulators.

Keywords: Multi modal locomotion, Flying robot, Linear quadratic regulator, Admittance control

ÖZ

MELEZ (ÇOK MODLU) BİR UÇAN ROBOT SINIFININ KAPALI ÇEVRİM DİNAMİĞİ

Battı, Mohamed Ismaıl

Doktora, Mühendislik Sistemlerinin Modellenmesi Tasarımı Bölümü
Tez Yöneticisi: Asst. Prof. Dr. Kutluk Bilge Arıkan
Ortak Tez Yöneticisi: Prof. Dr. Hüseyin Nafiz Alemdaroğlu

Ağustos 2020, 55 sayfa

Bu çalışmada, basit ve ileri seviyeden oluşan melez bir uçan robot sınıfı önerilmiştir. Her iki sistem için iki boyutlu uzayda doğrusal ve doğrusal olmayan modeller çıkarılmıştır. Doğrusal kuadratik regülatör temelli denetim sistemleri, askı durumu ve navigasyon senaryolarına yönelik olarak tasarlanmıştır. Benzetimlerde bozucu dış kuvvetler dikey kalkış, ileri uçuş ve iniş sırasında etki etmiştir. Senaryolar esnasında basit ve ileri seviye sistemlerin dinamik davranışlarının karşılaştırılmasının yanında her bir sistem için doğrusal ve doğrusal olmayan sistem cevapları da değerlendirilmiştir. Admitans tipi denetimcinin, zorlayıcı dış kuvvetlerin etki ettiği hallerde basit sisteminin kararlılığını sağladığı benzetimler ile sunulmuştur. Her iki sistem de kara-hava melez sistem olarak ve hava manipülatörü olarak kullanıma uygun olduğu sunulmuştur.

Anahtar Kelimeler: Çok modluhareket, Uçan robot, Doğrusal kuadratik regülatör, Admitans denetimi

DEDICATION

I dedicate this thesis to my parents and to my wife and children and to my brothers for their constant support and unconditional love.

ACKNOWLEDGMENTS

I am grateful to Allah SWT, the most powerful and the most merciful for His blessing of giving me this opportunity to complete this project successfully. Never forget Peace and Prayers to the Prophet, Muhammad s.a.w.

First, I would like to express my enormous gratitude to my two thesis supervisors, Asst. Prof. Dr. Kutluk Bilge Arıkanand Prof. Dr. Nafiz Alemdaroğlu, for their encouragement, guidance and advice continuous during my research study. Their wisdom and expert guidance have been indispensable in the elaboration of this thesis and without their efforts, I would not have had the support to finish this work. It was a pleasure to work under the supervision of these two true gentlemen.

I shall also thank to my committee members for oaring me their comments and suggestions to accomplish my work in appropriate way.

I would need more than a lifetime to thank all what my beloved wife, Fouzia Ben, Ziglam has made for me. She has worked a lot to make this possible. Without her, I would not have been capable to bring this to an end. This thesis is also hers.

Furthermore, the special thanks go to my parents, my friend Çağatay ÖZTÜRK and colleague, Alyaseh Askari, for their continuous encouragement and support. People like this are essential to make research possible.

Appreciation is also extended to all my friends. Their help was invaluable in particular periods of this work.

Lastly, I offer my regards and blessings to all of those who contributed to the emergence of this work for light, even by supplication.

TABLE OF CONTENTS

LIST OF TABLES

LIST OF FIGURES

LIST OF SYMBOLS/ABBREVIATIONS

F.....Motor Thrusts

m_1.....Mass of upper units

m_2.....Mass of link

m_3.....Mass of limb

I_1.....Moment of Inertia of hybrid robot

I_2.....Moment of Inertia of link

I_3.....Moment of Inertia of limb

a_{11} .....Length between Center of gravity and Propeller Unit

a_{12} .....Length between Center of gravity and joint B

a_2.....Length between Center of gravity and joint D

a_3.....Length between Center of gravity and joint G

θ_1.....Roll Angle

θ_2.....Rotational angle of the link

θ_3.....Rotational angle of the angle limb

T_1.....Torque of system's Joint

T_2.....Torque of system's Joint

F_1, F_2 .....Reaction Forces at the joint B

$F_{ex}F_{ey}$.....Reaction Forces of system's

F_3, F_4 .....Reaction Forces at the joint D

g.....Gravity

X_D, Y_D.....The desired coordinates of the trajectory

R_x, R_y .....The reference inputs

$\ddot{x}_C, \ddot{y}_C$ .....Accelerations of Basic on Center of Gravity of Basic system

$\ddot{x}_E, \ddot{y}_E$ .....Accelerations of Advanced on Center of Gravity of Advanced system

CHAPTER 1

INTRODUCTION

In the past few years, the design of multi-modal or hybrid robotic platforms has been emerging in robot science. These systems have inherited multiple styles of locomotion subsystems for the generation of motion. A hybrid locomotion mechanism results in being an effective and efficient system in various environments in comparison to an individual mode of locomotion. In robotics combining different systems with different locomotion systems may reveal an optimal solution for certain applications. The legged-wheeled type of hybrid robots is the most common type of multi-modal locomotion.

Besides the legged-wheeled locomotion, the hybrid system in [1] was designed as a micro air land robot which is capable of performing aerial and terrestrial locomotion. By the aid of the adaptive morphology, the wings are utilized as legs during the locomotion on ground. It performs transitions from flight to walking and in some situations, from walking to flight. In case of having an underactuated nature, integration of the actuation units becomes a challenge. In this aspect, a design analysis was performed to determine the optimal integration of flight and ground locomotion mechanisms in [2]. Another study combines wheeled ground movement with the rotary-wing flight capabilities, which have the ability to provide the best features of both helicopters and ground vehicles [3]. The design of multi-propeller multifunction aerial robot (MMAR) served to increase the agility in addition to the functionality by the aid of the hybrid locomotion system. The dynamics of hybrid flying-walking locomotion is rather complex since due to the need of contacting with the environment [4]. Another hybrid flying robot, FSTAR, is equipped with a sprawling mechanism and propellers to crawl and fly using the same motors. The combined capabilities allow FSTAR to fly over obstacles or crawl underneath them and move inside pipes. The robot can reduce its width to crawl in confined spaces or underneath obstacles while remaining in contact with the ground [5]. A novel robotic system

integrating walking and flying abilities was designed for the inspection and maintenance purposes. To compensate the vibration, the flexible robot arm was modeled by finite element method [6] and Linear Quadratic Gaussian (LQG) based controller was designed to control the system. The Hybrid exploration robot (H.E.R.A.L.D.) presents a new solution for air and land deployment and it is composed of three agile, lightweight robots to travel over large obstacles by air, but can also travel through debris [7].

Jumping provides another distinct solution to locomotive in air for a short time interval. Flying jumping multi-modal locomotion is studied in [8] to mimic the locomotion of locusts. They showed that the use of flapping wings and jumping enabled the bio-mimicked robot to have stable landing as the locusts do. Zhao et al. in [9] presented a novel robot that can run and jump if necessary. The stability in air is maintained by the aid of an actuated tail. This integration provides stable locomotion in air for a limited/short time interval. The system cannot hover in the air. However, the design in [10] has the ability to hover in air by twin rotary wing actuation system in tandem configuration. The pitch stability in air is guaranteed by the actuated wheels that generate required torque in pitch axis. The author designed a 2-wheeled twin rotor system and a robust control system that satisfies the robust stability in transition mode, i.e., ground-air transition. An underactuated walking-flying type hybrid robot is designed in [11]. A quadcopter is equipped with a passive-dynamic leg system. This system does not require the use of legs in air motion.

Hybrid locomotion robots that utilize legged ground locomotion and rotary-wing flight hold great promise for increasing the mobility of robots. Such robots perform better than ground-only robots in that a flight mode is available for use when otherwise obstacles are confronted. The research in this article focuses on the hybrid robotic system, especially in terms of modeling and control. In this study, two versions of the hybrid system are examined in flight phase. The first one is the Basic System and the second is the Advanced System with one more additional joint in the leg, Figure 1.1

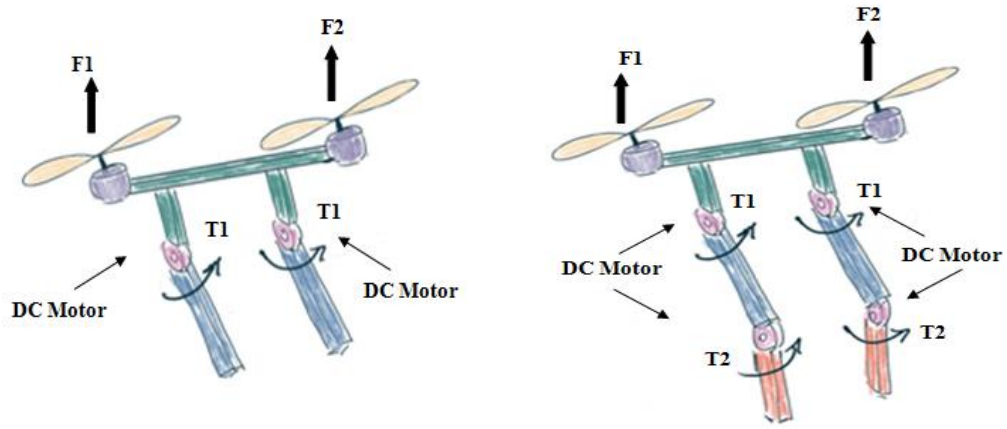

a) Conceptual Basic System b) Conceptual Advanced System

Figure 1.1 Hybrid Air-Ground Robotic System

Both of the versions are underactuated. The basic system has four degrees of freedom (DoF) and two degrees of actuation (DoA) in 2D space. The advanced one has five DoF and three DoA. Both of the versions are underactuated. The main contributions of the study are listed as below.

- The proposed system is an underactuated robotic system that requires the use of legs in the air to maintain stability and navigation. This is an uncommon multi-modal approach that allocates the control to all the actuators of the system.

- Two versions are discussed and compared in terms of closed loop dynamical performances. The basic system is already controllable in the air. The advanced system has an additional degree of freedom and degree of actuation. The inter-version differences are analyzed as similar control systems are applied to both of the versions.

- For each version, the responses of linearized and nonlinear models are analyzed, as well. The control system is designed based on the linearized model. The designed control system is applied on the nonlinear model, too. The closed loop responses are compared and discussed.

- The control systems are designed for two main scenarios. The first scenario assumes that the systems are controlled in the hovering mode. The second one focuses on the position control as the systems track the given reference positions. Two sub-scenarios are studied during the position control. Firstly, no external/disturbance forces are applied. However, in the second phase, external/disturbance forces are applied, and the performances are discussed. In this phase, firstly the robustness of the designed position control systems is discussed and then the admittance controllers are designed and simulated to present the effectiveness of interacting the external forces instead of rejecting them.

CHAPTER 2

METHODOLOGY

The nonlinear dynamical models are derived at first. The control systems are designed using linearized models. Figure 2.1 shows the simplified physical models in X-Y plane.

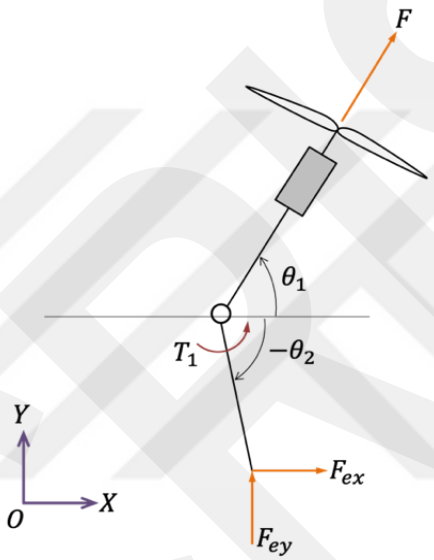

a) Basic System

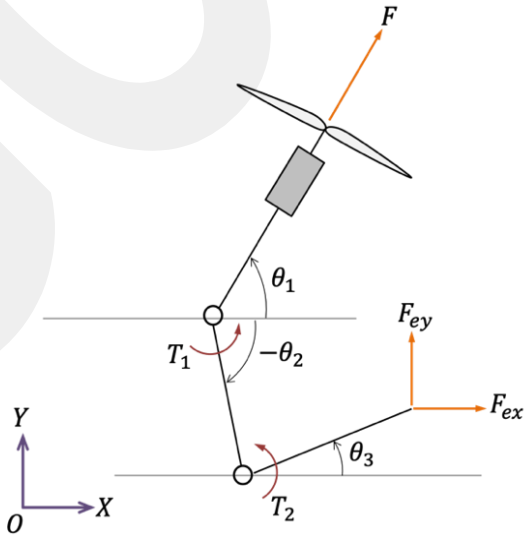

b) Advanced System

Figure 2.1 Hybrid Robots – Basic and Advanced Platforms

2.1 Mathematical Modeling

The dynamical models for both versions are derived using the free body diagrams. It is assumed that the robots are locomoting in 2D space. The actuators are assumed to be ideal. The nonlinear models are simulated in MatLab/Simulink. The linearized models are utilized to design linear state-feedback controllers. Linear control systems are applied to the nonlinear system models, as well. The responses of basic and advanced systems are evaluated using mathematical measures. The main scenarios are *a*) regulating in the hovering mode and *b*) tracking control for navigation in 2D space. The nonlinear dynamical model for the basic system is obtained using the following schematics in Figure 2.3*A* and *C* represent the mass center of the main chassis and the limb of the system respectively.

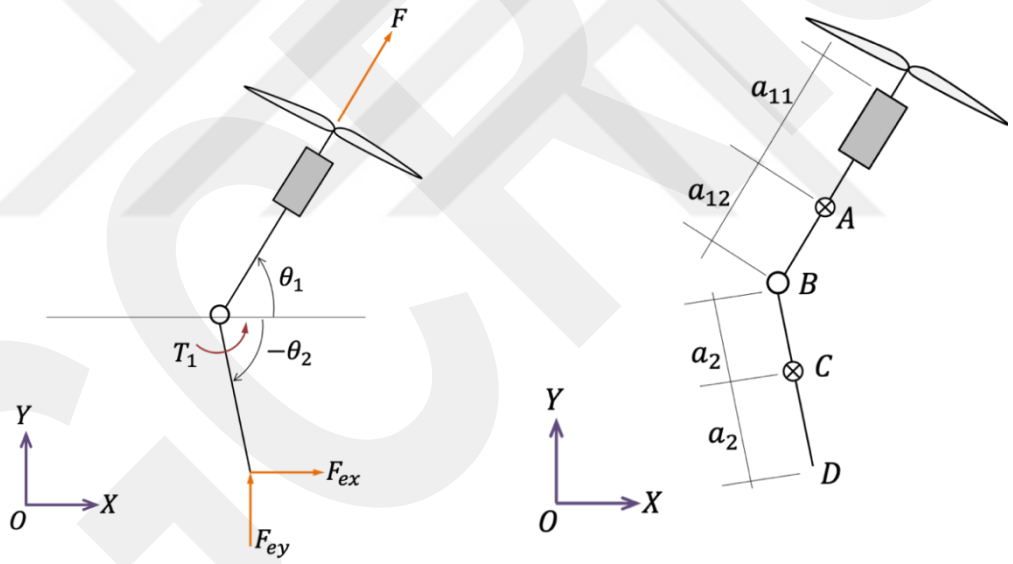

Figure 2.2 Schematics of the Basic System

The position, velocity and the acceleration vectors of point A are given as follows.

$$\vec{r}_A = x\vec{i} + y\vec{j} \quad (1)$$

$$\vec{V}_A = \dot{x}\vec{i} + \dot{y}\vec{j} \quad (2)$$

$$\vec{a}_A = \ddot{x}\vec{i} + \ddot{y}\vec{j} \quad (3)$$

Similarly, the position, velocity and the acceleration vectors of point C are given as follows.

$$\vec{r}_C = \vec{r}_A - (a_{12}\cos\theta_1\vec{i} + a_{12}\sin\theta_1\vec{j}) + (a_2\cos\theta_2\vec{i} + a_2\sin\theta_2\vec{j}) \quad (4)$$

$$\vec{V}_C = \vec{V}_A - a_{12}\dot{\theta}_1\left(-\sin\theta_1\vec{i} + \cos\theta_1\vec{j}\right) + a_2\dot{\theta}_2(-\sin\theta_2\vec{i} + \cos\theta_2\vec{j}) \quad (5)$$

$$\vec{a}_C = \vec{a}_A - a_{12}\ddot{\theta}_1\left(-\sin\theta_1\vec{i} + \cos\theta_1\vec{j}\right) + a_{12}\dot{\theta}_1^2(\cos\theta_1\vec{i} + \sin\theta_1\vec{j}) + a_2\ddot{\theta}_2(-\sin\theta_2\vec{i} + \cos\theta_2\vec{j}) - a_2\dot{\theta}_2^2(\cos\theta_2\vec{i} + \sin\theta_2\vec{j}) \quad (6)$$

$$\vec{a}_C = \left(\ddot{x} + a_{12}\ddot{\theta}_1\sin\theta_1 + a_{12}\dot{\theta}_1^2\cos\theta_1 - a_2\ddot{\theta}_2\sin\theta_2 - a_2\dot{\theta}_2^2\cos\theta_2\right)\vec{i} + (\ddot{y} - a_{12}\ddot{\theta}_1\cos\theta_1 + a_{12}\dot{\theta}_1^2\sin\theta_1 + a_2\ddot{\theta}_2\cos\theta_2 - a_2\dot{\theta}_2^2\sin\theta_2)\,\vec{j} \quad (7)$$

The components of the acceleration of point *C* are given as below.

$$\ddot{x}_C = (\ddot{x} + a_{12}\ddot{\theta}_1\sin\theta_1 + a_{12}\dot{\theta}_1^2\cos\theta_1 - a_2\ddot{\theta}_2\sin\theta_2 - a_2\dot{\theta}_2^2\cos\theta_2) \quad (8)$$

$$\ddot{y}_C = (\ddot{y} - a_{12}\ddot{\theta}_1\cos\theta_1 + a_{12}\dot{\theta}_1^2\sin\theta_1 + a_2\ddot{\theta}_2\cos\theta_2 - a_2\dot{\theta}_2^2\sin\theta_2) \quad (9)$$

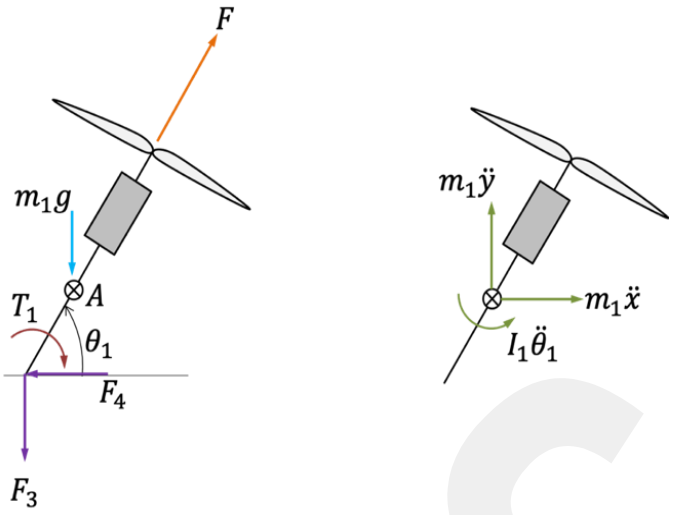

(a) FBD of the Chassis

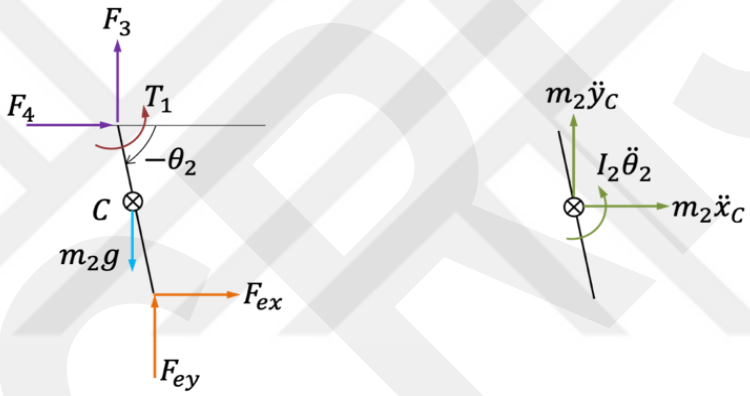

(b) FBD of the Limb

Figure 2.3 Free Body Diagrams (FBDs) of the Basic System

Using free-body diagrams in Figures 2.3 a and b, the following equations of motion are derived.

$$F_{ex} + F_4 = m_2\ddot{x}_C \quad (11)$$

$$F_{ey} + F_3 - m_2g = m_2\ddot{y}_2 \quad (12)$$

$$F_{ey}a_2\cos(-\theta_2) + F_{ex}a_2\sin(-\theta_2) - F_3a_2\cos(-\theta_2) - F_4a_2\sin(-\theta_2) + T_1 = I_2\ddot{\theta}_2 \quad (13)$$

$$-F_4 + F\cos\theta_1 = m_1\ddot{x} \quad (14)$$

$$-F_3 + F\sin\theta_1 - m_1g = m_1\ddot{y} \quad (15)$$

$$F_3a_{12}\cos\theta_1 - F_4a_{12}\sin\theta_1 - T_1 = I_1\ddot{\theta}_1 \quad (16)$$

These six equations of motion are solved to find the reaction forces$F_3$and F_4 and for the accelerations $\ddot{x}$, $\ddot{y}$, $\ddot{\theta}_1$, and $\ddot{\theta}_2$ Nonlinear terms for the accelerations are used in the nonlinear state-space model.

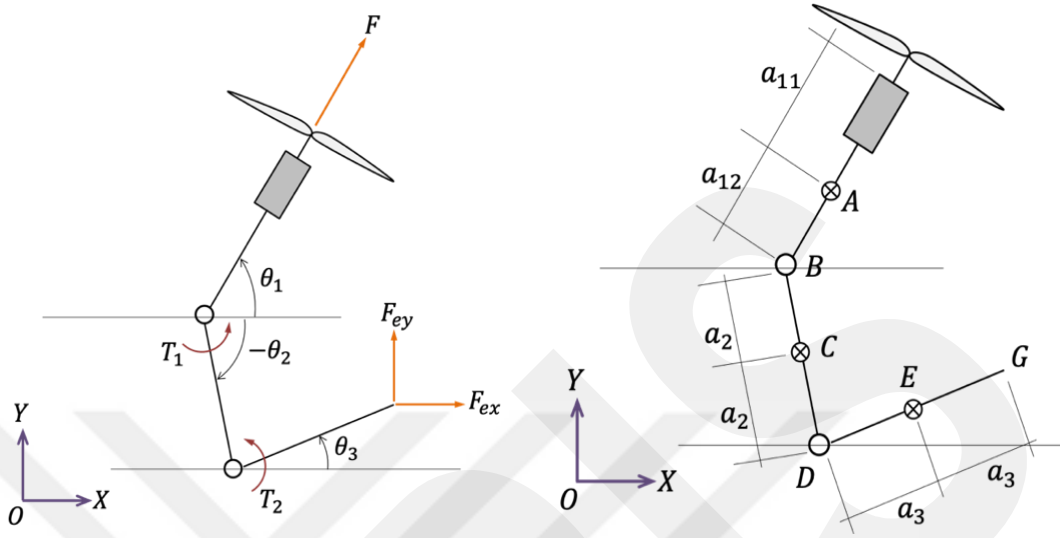

Figure 2.4Schematics of the Advanced System

The nonlinear dynamical model for the advanced system is obtained using the schematics in Figures 2.4A, C and E represent the mass center of the main chassis and the limbs of the system respectively. The position, velocity and the acceleration vectors of point *E* are given as follows.

$$\vec{r}_E = \vec{r}_C + (a_2\cos\theta_2\vec{i} + a_2\sin\theta_2\vec{j}) + (a_3\cos\theta_3\vec{i} + a_3\sin\theta_3\sin\theta_3\vec{j}) \quad (17)$$

$$\vec{V}_E = \vec{V}_C + a_2\dot{\theta}_2(-\sin\theta_2\vec{i} + \cos\theta_2\vec{j}) + a_3\dot{\theta}_3(-\sin\theta_3\vec{i} + \cos\theta_3\vec{j}) \quad (18)$$

$$\vec{a}_E = \vec{a}_c + a_2\ddot{\theta}_2(-\sin\theta_2\vec{i} + \cos\theta_2\vec{j}) - a_2\dot{\theta}_2^2(\cos\theta_2\vec{i} + \sin\theta_2\vec{j}) + a_3\ddot{\theta}_3(-\sin\theta_2\vec{i} + \cos\theta_3\vec{j}) - a_3\ddot{\theta}_3(-\sin\theta_3\vec{i} + \cos\theta_3\vec{j}) - a_3\dot{\theta}_3^2(\cos\theta_3\vec{i} + \sin\theta_3 j) \quad (19)$$

The components of the acceleration of point E are given as below.

$$\ddot{x}_E = (\ddot{x} + a_{12}\ddot{\theta}_1\sin\theta_1 + a_{12}\dot{\theta}_1^2\cos\theta_1 - 2a_2\ddot{\theta}_2\sin\theta_2 - 2a_2\dot{\theta}_2^2\cos\theta_2 - a_3\ddot{\theta}_3\sin\theta_3 - a_3\dot{\theta}_3^2\cos\theta_3) \quad (20)$$

$$\ddot{y}_E = (\ddot{y} - a_{12}\ddot{\theta}_1\cos\theta_1 + a_{12}\dot{\theta}_1^2\sin\theta_1 + 2a_2\ddot{\theta}_2\cos\theta_2 - 2a_2\dot{\theta}_2^2\sin\theta_2 + a_3\ddot{\theta}_3\cos\theta_3 - a_3\dot{\theta}_3^2\sin\theta_3) \quad (21)$$

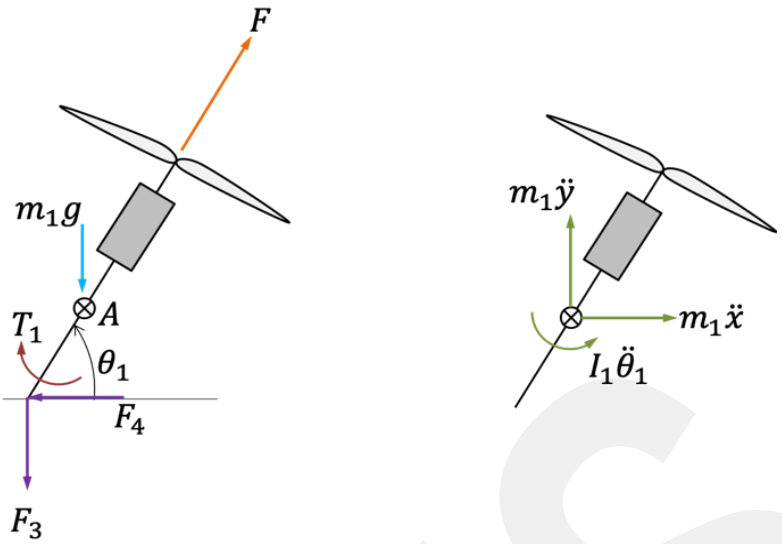

a) FBD of the Chassis

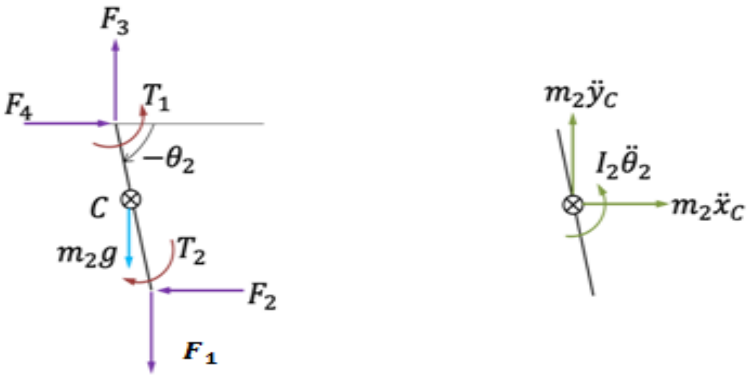

b) FBD of the Proximal Limb

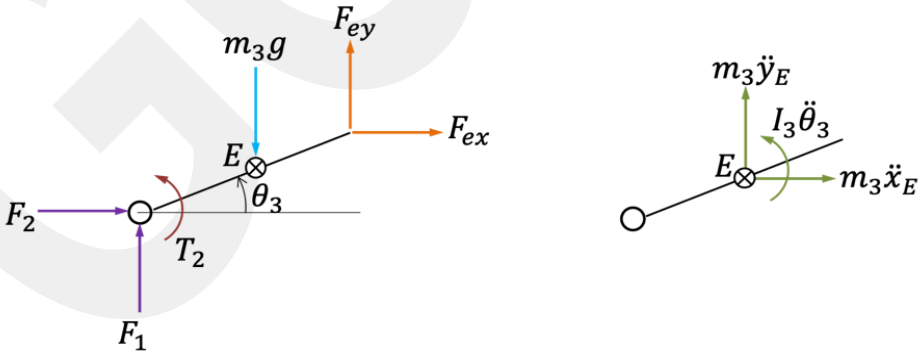

c) FBD of the Distal Limb

Figure 2.5 Free Body Diagrams of the Advanced System

Using free-body diagrams in Figure 2.5, the following equations of motion are derived.

$$F_2 + F_{ex} = m_3\ddot{x}_E \tag{22}$$

$$F_1 + F_{ey} - m_3 g = m_3\ddot{y}_E \tag{23}$$

$$-F_1 a_3 \cos\theta_3 + F_2 a_3 \sin\theta_3 + F_{ey} a_3 \cos\theta_3 - F_{ex} a_3 \sin\theta_3 + T_2 = I_3\ddot{\theta}_3 \tag{24}$$

$$-F_2 + F_4 = m_2\ddot{x}_C \tag{25}$$

$$-F_1 + F_3 - m_2 g = m_2\ddot{y}_C \tag{26}$$

$$-F_1 a_2 \cos(-\theta_2) - F_2 a_2 \sin(-\theta_2) - F_3 a_2 \cos(-\theta_2) - F_4 a_2 \sin(-\theta_2) + T_1 - T_2 = I_2\ddot{\theta}_2 \tag{30}$$

$$-F_4 + F\cos\theta_1 = m_1\ddot{x} \tag{28}$$

$$-F_3 + F\sin\theta_1 - m_1 g = m_1\ddot{y} \tag{29}$$

$$F_3 a_{12} \cos\theta_1 - F_4 a_{12} \sin\theta_1 - T_1 = I_1\ddot{\theta}_1 \tag{30}$$

These nine equations of motion are solved to find the reaction forces F_1, F_2, F_3, and F_4 and for the accelerations $\ddot{x}$, $\ddot{y}$, $\ddot{\theta}_1$, $\ddot{\theta}_2$ and $\ddot{\theta}_3$. Nonlinear terms for the accelerations are used in the nonlinear state-space model.

CHAPTER 3

CONTROLLER DESIGN

Linear quadratic regulator design is used as the basis to compare the dynamic performances of the basic and advanced versions. Firstly, the systems are regulated during hovering. The linearized model is utilized to design the state-feedback controllers. Both linear and nonlinear simulations are performed using the linearized and nonlinear models. The state vectors for the basic and advanced systems are given respectively.

$$x_b = \left[X, \dot{X}, Y, \dot{Y}, \theta_1, \dot{\theta}_1, \theta_2, \dot{\theta}_2\right]^T \tag{31}$$

$$x_a = \left[X, \dot{X}, Y, \dot{Y}, \theta_1, \dot{\theta}_1, \theta_2, \dot{\theta}_2, \theta_3, \dot{\theta}_3\right]^T \tag{32}$$

The input vectors for the basic and advanced systems are given respectively.

$$u_b = \left[F, T_1, F_{ex}, F_{ey}\right]^T \tag{33}$$

$$u_a = \left[F, T_1, T_2, F_{ex}, F_{ey}\right]^T \tag{34}$$

Nonlinear state equations are derived based on the equations of motion which are derived in the previous section.

$$\dot{x}_b = f_b(x_b, u_b)$$

$$\dot{x}_a = f_a(x_a, u_a)$$

The control systems are designed on the linearized state space models of the basic and advanced systems. The linearization is performed as below.

$$\partial\dot{x}_b = \frac{\partial f_b}{\partial x_b}\Big|_{x_{bn}} \partial x_b + \frac{\partial f_b}{\partial u_b}\Big|_{u_{bn}} \partial u_b \tag{35}$$

$$\partial \dot{x}_a = \frac{\partial f_a}{\partial x_a}\Big|_{x_{an}} \partial x_a + \frac{\partial f_a}{\partial u_a}\Big|_{u_{an}} \partial u_a \tag{36}$$

x_{bn} and x_{an} are the nominal state vectors to represent the operating point for the linearization of the basic and advanced systems respectively. u_{bn} and u_{an} are the nominal input vectors to represent the operating point for the linearization of the basic and advanced systems respectively. The linearization reveals the following (LTI) linear time in variant models for the basic and advanced systems. It is assumed that all states are measured and used for the feedback control.

$$\dot{x}_b = A_b x_b + B_b u_b \tag{37}$$

$$\dot{x}_a = A_a x_a + B_a u_a \tag{38}$$

where

$$A_b = \frac{\partial f_b}{\partial x_b}\Big|_{x_{bn}} \text{ and} B_b = \frac{\partial f_b}{\partial u_b}\Big|_{u_{bn}} \tag{39}$$

$$A_a = \frac{\partial f_a}{\partial x_a}\Big|_{x_{an}} \text{ and} B_a = \frac{\partial f_a}{\partial u_a}\Big|_{u_{an}} \tag{40}$$

The controllability of the systems are presented by the rank of the controllability matrices of the linearized systems using the (A_b, B_b) and (A_a, B_a) pairs. The controllability matrices are defined as follows.

$$\mathcal{C}_b = [B_b \quad \dots \quad A_b^7 B_b] \tag{41}$$

$$\mathcal{C}_a = [B_a \quad \dots \quad A_a^9 B_a] \tag{42}$$

It is found that the controllability matrices are full rank. Therefore, both of the configurations are controllable. However, a more detailed analysis is performed by the singular value decomposition of the controllability gramians [26]. The controllability gramians for the basic and advanced systems are given as follows.

$$W_b = \mathcal{C}_b \mathcal{C}_b^T \tag{43}$$

$$W_a = \mathcal{C}_a \mathcal{C}_a^T \tag{44}$$

Singular value decompositions of the abovementioned gramians are shown as below.

$$W_b = U_b \Sigma_b U_b^T \tag{45}$$

$$W_a = U_a \Sigma_a U_a^T \tag{46}$$

U_b and U_a are 8 × 8 and 10 × 10 matrices including singular vectors. Σ_b and $\Sigma_a$are the diagonal matrices with the singular values σ_{bi} and s σ_{ai} on the diagonal. σ_{b8} and σ_{a10} are the smallest singular values for the basic and advanced systems. The corresponding singular vectors in U_b and U_a show the states that are difficult to control and accordingly the directions in the state-space that requires high amount of control energy [26].

In order to assess the performances of the proposed systems, mainly 2 scenarios and corresponding control algorithms are studied. Firstly, the systems are controlled in the hovering condition by the aid of linear quadratic regulators (LQR). Subsequently, LQR-servo type controllers are used to track a reference path in 2D navigation. Finally, the basic and advanced system performances are evaluated as they are controlled by an admittance control while external interaction forces (F_{ex}, F_{ey}) are applied.

3.1. LQR Design for Hovering

The LQR design is made to minimize the following cost function.

$$J_k = \int_0^\infty (x_k^T Q_k x_k + u_k^T R_k u_k) dt, \tag{47}$$

$u_k = -K_k x_k$ where $k = \{b, a\}$

Nonlinear and linearized models are built in Simulink and the designed LQR is applied on both nonlinear and linearized models. Figure 3.1 presents the schematics of the regulators.

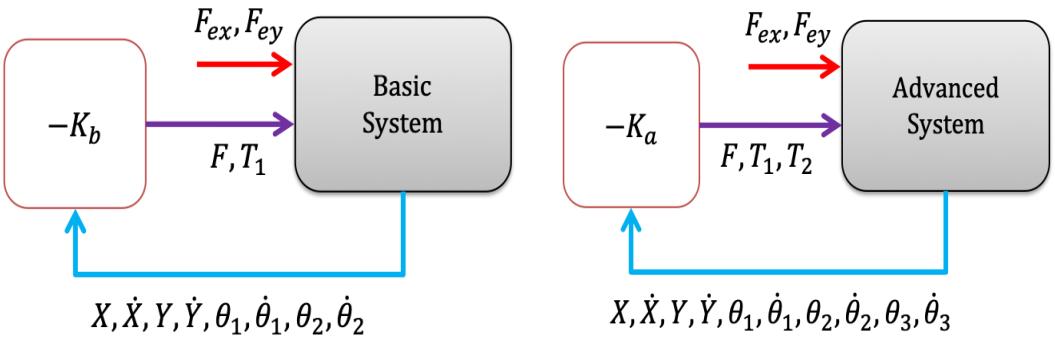

Figure 3.1 LQR for the basic system (right) and advanced system (left)

3.2. LQR-Servo Design for Navigation

The LQR-Servo is designed to minimize the following cost function for the extended system with error states.

$$J_k = \int_0^\infty \left(\bar{x}_k^T Q_k \bar{x}_k + u_k^T R_k u_k\right) dt, \tag{48}$$

$$u_k = -[K_k \quad K_k^I]\bar{x}_k, \text{ where } k = \{b, a\}$$

The extended state vector, $\bar{x}_k$, is defined as follows.

$$\bar{x}_k = \begin{bmatrix} x_k \\ \int_0^t e(\tau)\, d\tau \end{bmatrix}, \text{where } e = \begin{bmatrix} R_X - x \\ R_Y - y \end{bmatrix}$$

The extended states pace model is given as below.

$$\dot{\bar{x}}_k = \bar{A}_k \bar{x}_k + \bar{B}_k u_k + \begin{bmatrix} 0 \\ \text{eye}(2,2) \end{bmatrix} \begin{bmatrix} R_X \\ R_Y \end{bmatrix} \tag{49}$$

$$y_k = \begin{bmatrix} X \\ Y \end{bmatrix} = C_k \bar{x}_k + D_k u_k \tag{50}$$

$\bar{A}_k$ and $\bar{B}_k$ are defined as

$$\bar{A}_k = \begin{bmatrix} A_k & 0 \\ -C_k & 0 \end{bmatrix}, \bar{B}_k = \begin{bmatrix} B_k \\ 0 \end{bmatrix}$$

Zero matrices in the abovementioned model are defined with the appropriate sizes. Nonlinear and linearized models are built in Simulink and the designed LQR is applied on both nonlinear and linearized models. Figure 3.2 presents the schematics of the LQR-servo type of control systems.

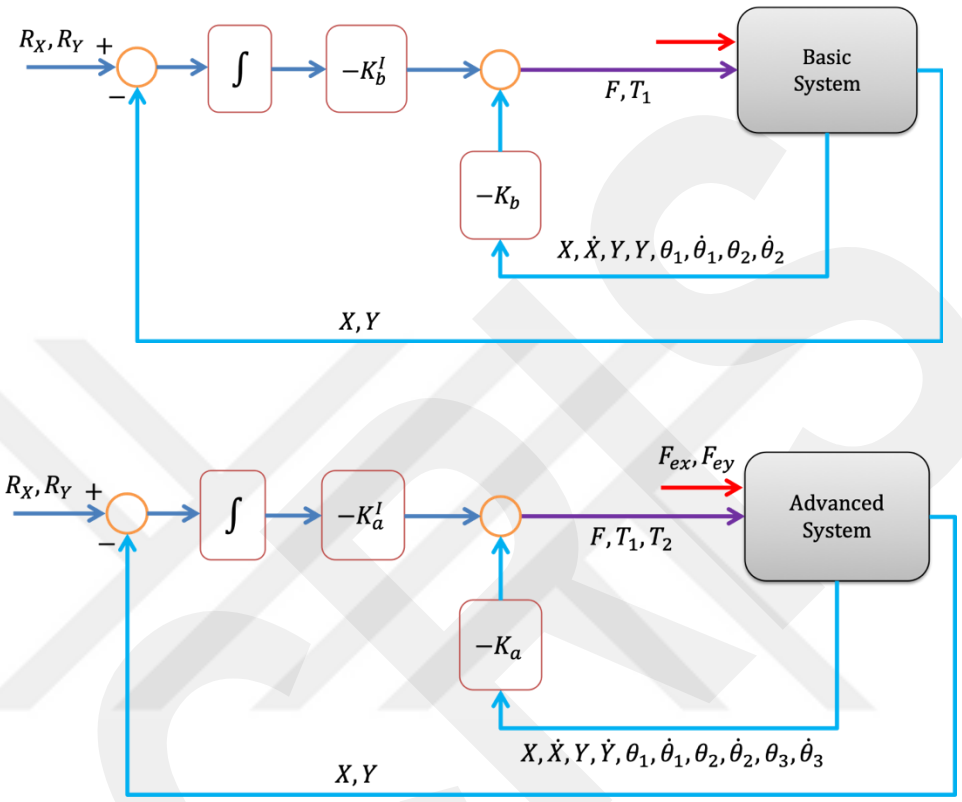

Figure 3.2 LQR-Servo Controllers for the basic system (top) and advanced system (bottom)

3.3. Admittance Control for Interaction during Navigation

The external forces are applied as the LQR-Servo control systems are implemented for navigation. This control architecture is acting to reject the external forces treating them as disturbance inputs. However, this may lead to unstable responses. Admittance control provides another way of action that utilizes interaction rather than rejecting the external forces [25]. Figure 3.3 presents the schematics of the admittance control implemented with the LQR-Servo control architecture. Admittance control modifies the reference inputs for the trajectory using a virtual mass-spring-damper system. It

assumed that the interaction force is applied at the end of the distal limb and it is measured by the aid of a force sensor.

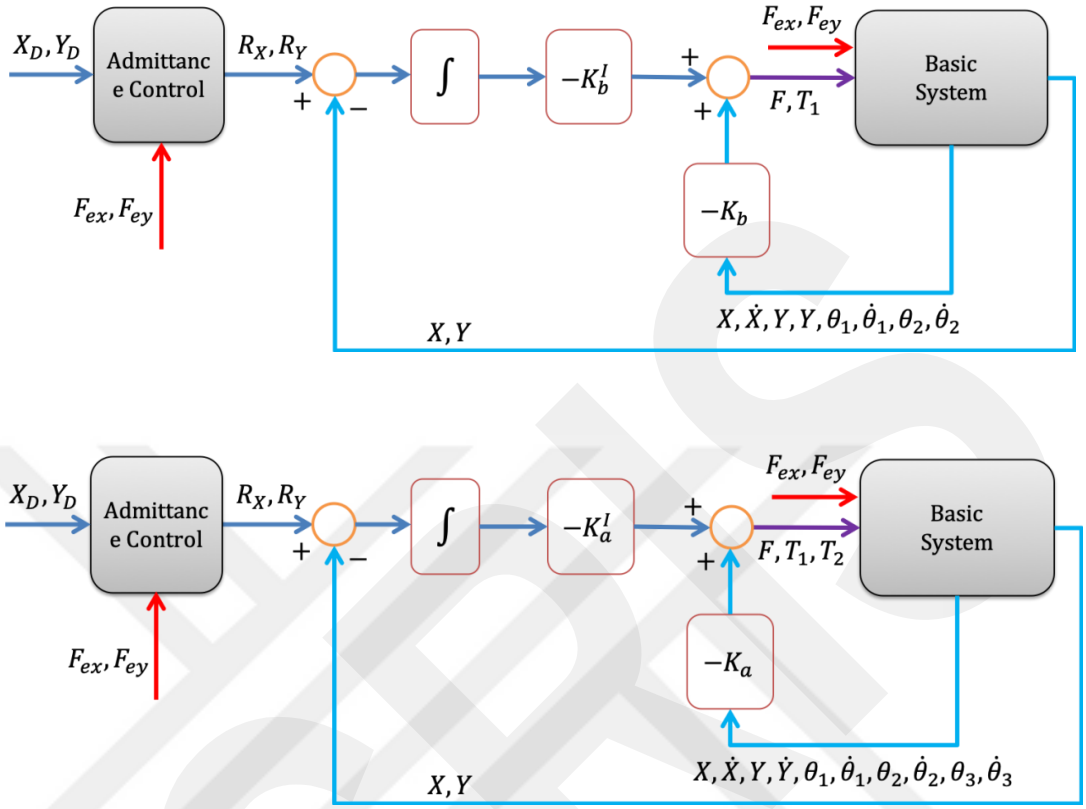

Figure 3.3 Admittance Controllers for the basic system (top)
and advanced system (bottom)

The reference inputs R_X and R_Y are obtained as the solutions of the following equations of motion that define the system in Figure 3.4. X_D and Y_D are the desired coordinates of the trajectory. m_v, b_v, and k_v are the virtual mass, damping coefficient, and the stiffness coefficient respectively.

$$m_v\ddot{R}_X + b_v\dot{R}_X + k_vR_X = b_v\dot{X}_D + k_vX_D + F_{ex} \quad (51)$$

$$m_v\ddot{R}_Y + b_v\dot{R}_Y + k_vR_Y = b_v\dot{Y}_D + k_vY_D + F_{ey} \quad (52)$$

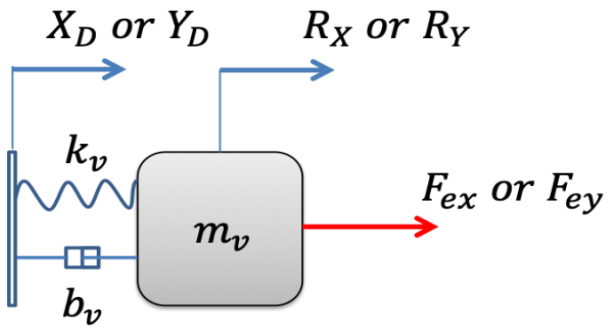

Figure 3.4 Virtual Mass-Spring-Damper System

CHAPTER 4

SIMULATIONS

The nonlinear and the linearized models for the basic and advanced systems are simulated in MatLab/Simulink. Firstly, the simulations are performed for the hovering case. Then the navigation control is simulated.

4.1 Simulations for Hovering Control

$$x_{b\_nominal} = \left[0, 0, 2, 0, \frac{\pi}{2}, 0, -\frac{\pi}{2}, 0\right]^T$$

The nominal input vector for the linearization is given as below.

$$u_{b\_nominal} = [(m_1 + m_2)g, 0, 0, 0]^T$$

The following weighting matrices are used to design the LQR for the basic system.

$$Q_b = 50\ \text{eye}(8, 8)$$

$$R_b = 300\ \text{eye}(2, 2)$$

eye(8, 8) and eye(2, 2) are 8 × 8 and 2 × 2 identity matrices.

The initial conditions for the state variables are given as below.

$$x_b(0) = \left[1, 0, -0.5, 0, \frac{40\pi}{180}, 0, 0, 0\right]^T$$

Similarly, the nominal state vector used for the linearization of the advanced system is given as follows.

$$x_{a\_nominal} = \left[0, 0, 2, 0, \frac{\pi}{2}, 0, -\frac{\pi}{2}, 0, -\frac{\pi}{2}, 0\right]^T$$

The nominal input vector for the linearization is

$$u_{a\_nominal} = [(m_1 + m_2 + m_3)g, 0, 0, 0, 0]^T$$

In order to compare with the response of the basic system, similar weighting matrices are used to design the LQR for the advanced system.

$$Q_a = 50\ \text{eye}(10, 10)$$

$$R_a = 300\ \text{eye}(3, 3)$$

eye (10, 10) and eye (3, 3) are 10 × 10 and 3 × 3 identity matrices

Similar to the basic system, the initial conditions for the state variables are given as below. Zero initial condition is given for the distal limb orientation, θ_3, similar to θ_2.

$$x_a(0) = \left[1, 0, -0.5, 0, \frac{40\pi}{180}, 0, 0, 0, 0, 0\right]^T$$

Figure 4.1 presents the system responses and Figure 4.2 shows the control inputs for the basic and advanced systems.

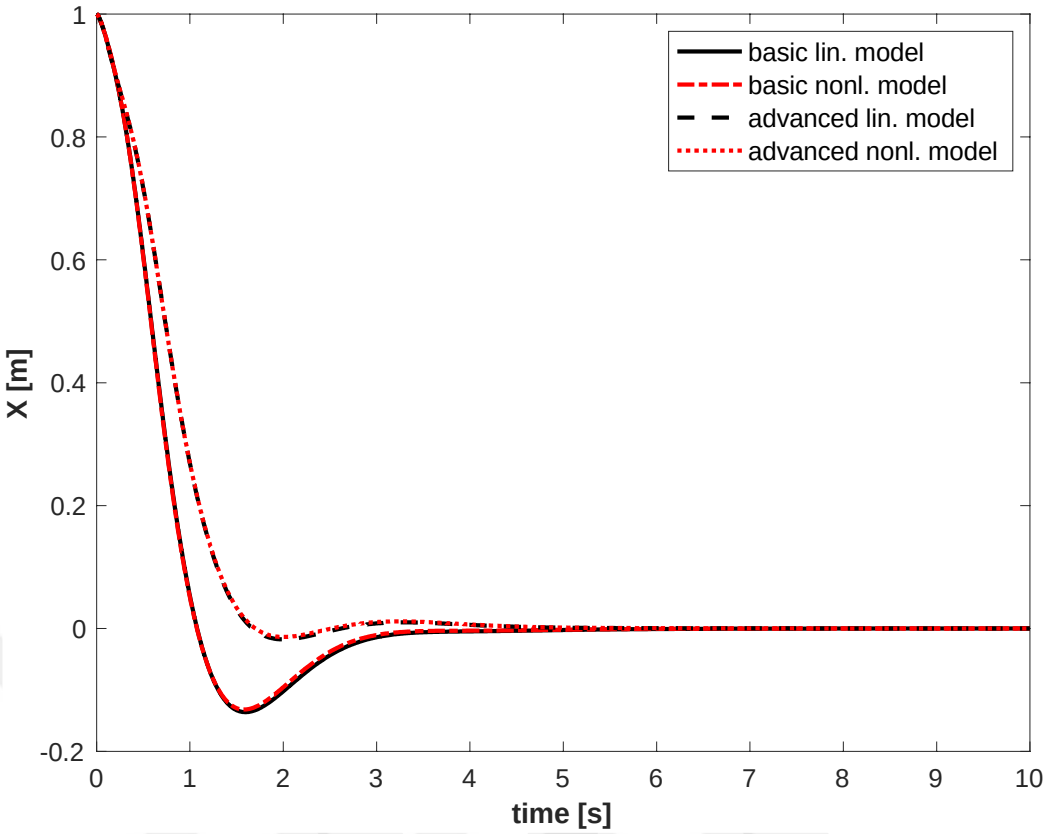
basic lin. model
basic nonl. model
advanced lin. model
advanced nonl. model
X [m]
time [s]
1
0.8
0.6
0.4
0.2
0
-0.2
0
1
2
3
4
5
6
7
8
9
10

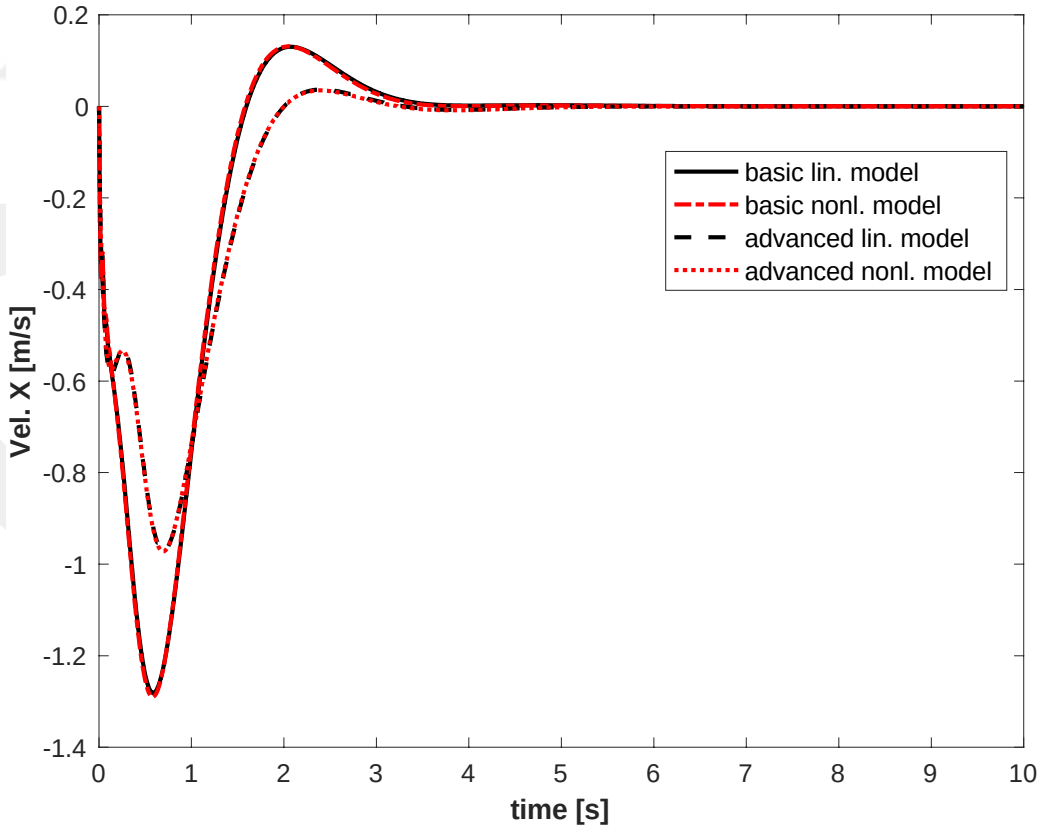
basic lin. model
basic nonl. model
advanced lin. model
advanced nonl. model
Vel. X [m/s]
time [s]
0.2
0
-0.2
-0.4
-0.6
-0.8
-1
-1.2
-1.4
0
1
2
3
4
5
6
7
8
9
10

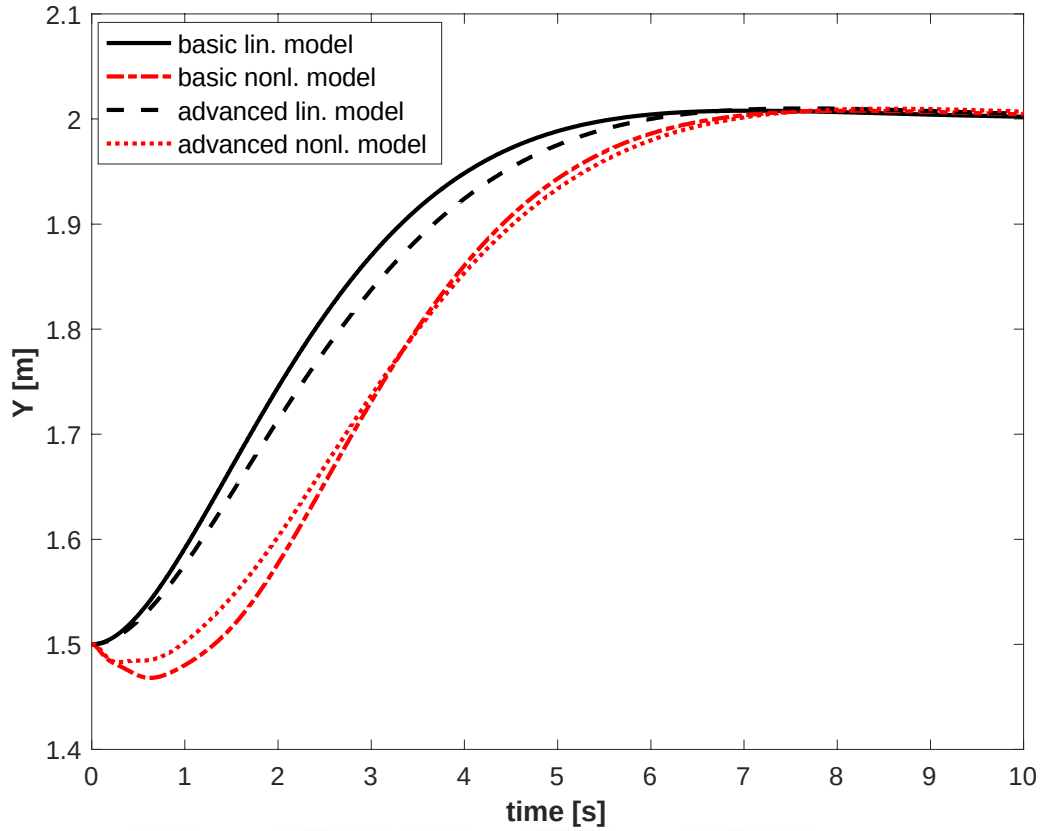
basic lin. model
basic nonl. model
advanced lin. model
advanced nonl. model
Y [m]
time [s]
2.1
2
1.9
1.8
1.7
1.6
1.5
1.4
0
1
2
3
4
5
6
7
8
9
10

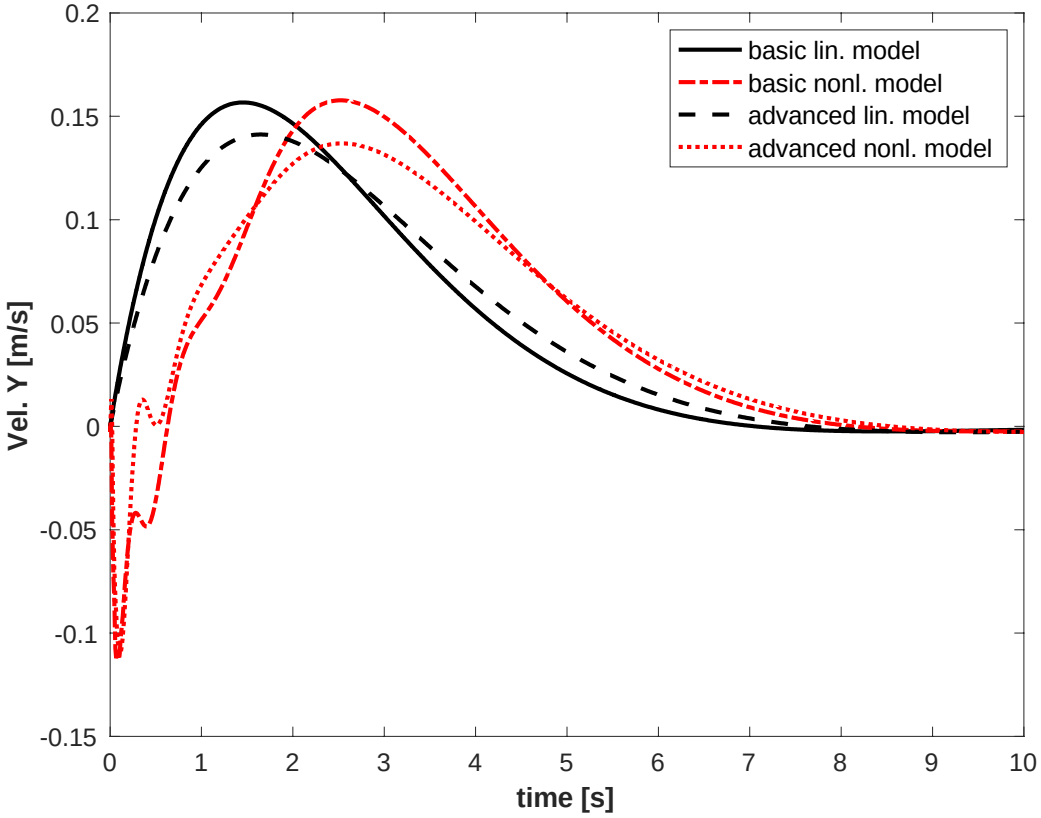
basic lin. model
basic nonl. model
advanced lin. model
advanced nonl. model
Vel. Y [m/s]
time [s]
0.2
0.15
0.1
0.05
0
-0.05
-0.1
-0.15
0
1
2
3
4
5
6
7
8
9
10

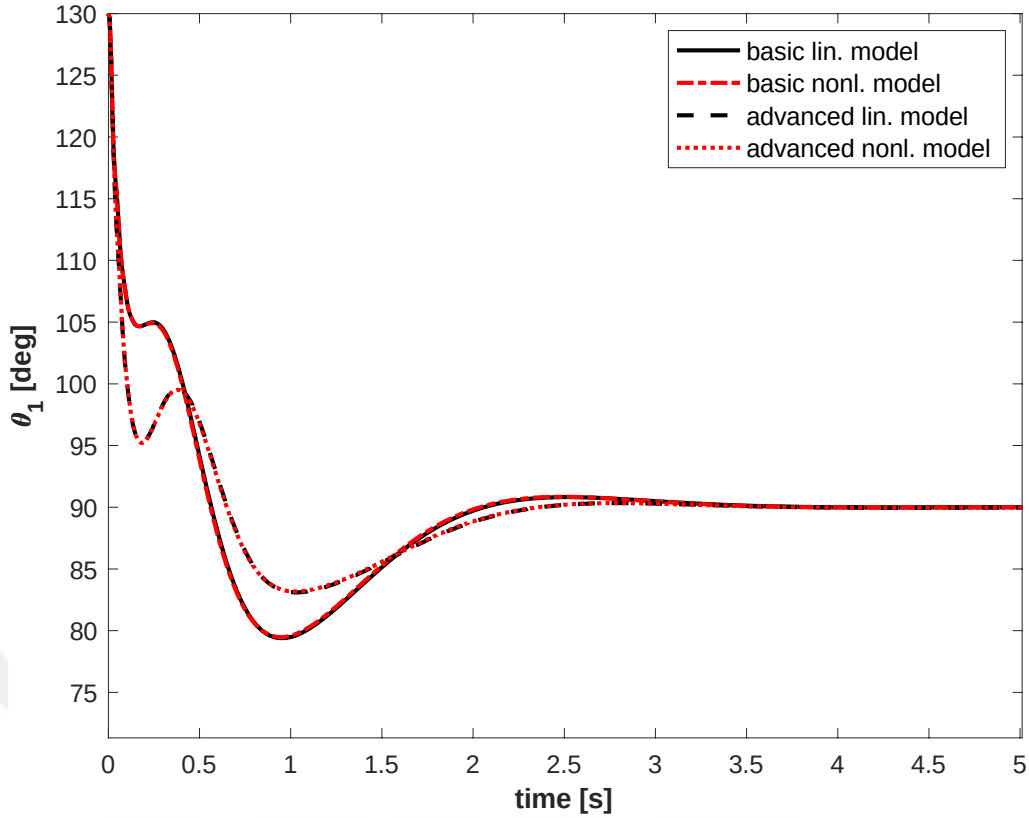
basic lin. model
basic nonl. model
advanced lin. model
advanced nonl. model
θ_1 [deg]
time [s]

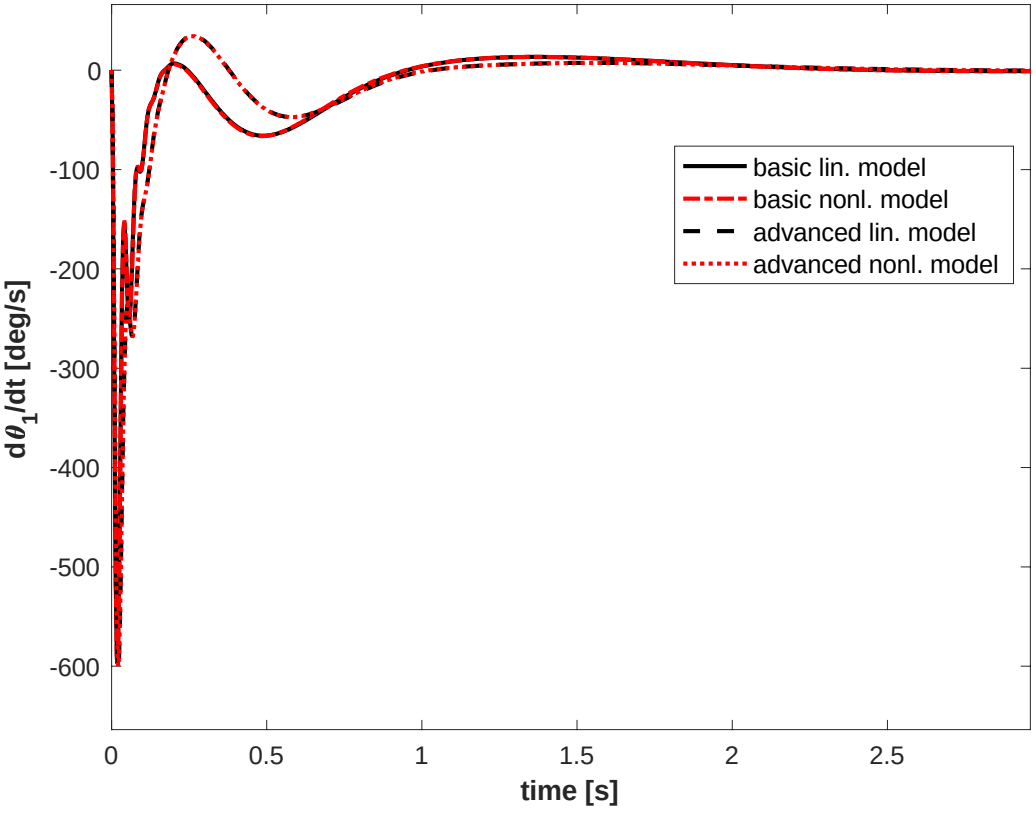
basic lin. model
basic nonl. model
advanced lin. model
advanced nonl. model
dθ_1/dt [deg/s]
time [s]

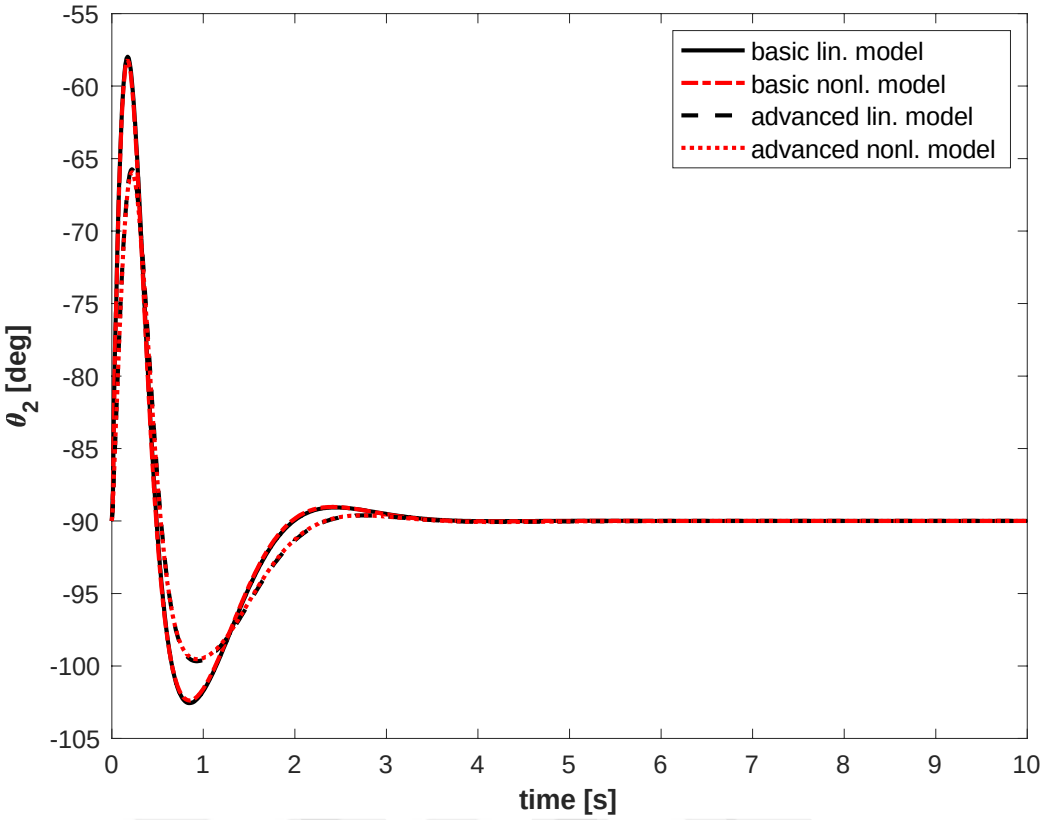
basic lin. model
basic nonl. model
advanced lin. model
advanced nonl. model
θ2 [deg]
time [s]

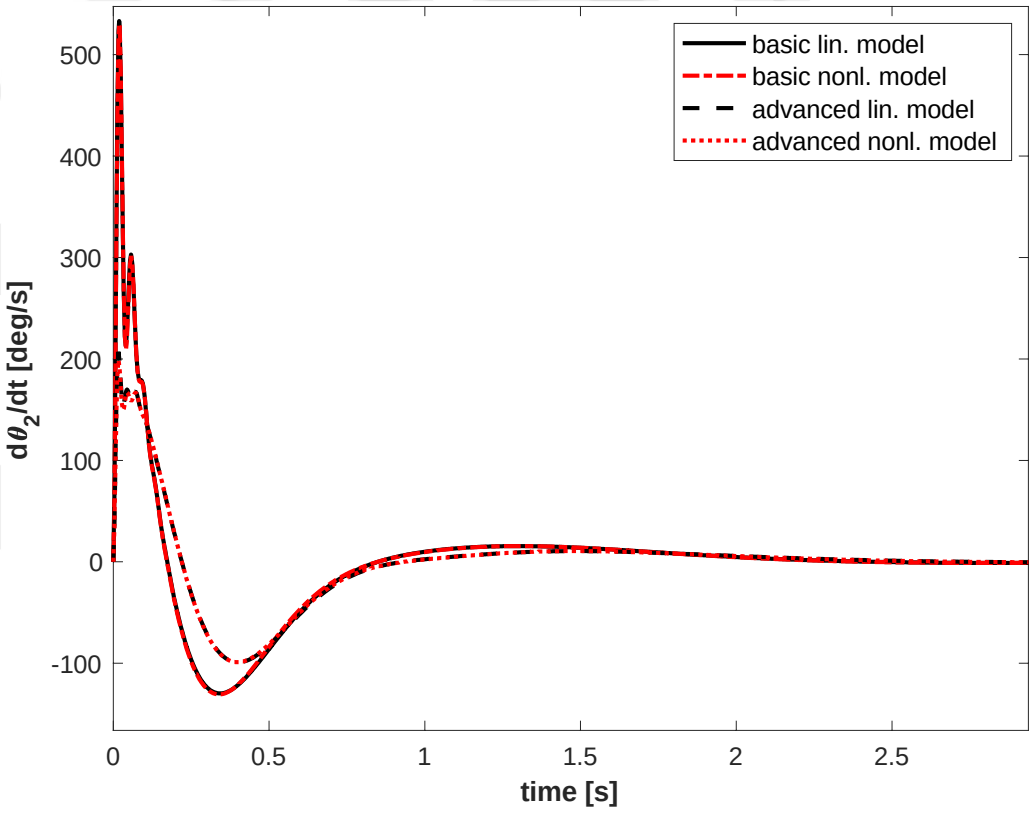
basic lin. model
basic nonl. model
advanced lin. model
advanced nonl. model
dθ2/dt [deg/s]
time [s]

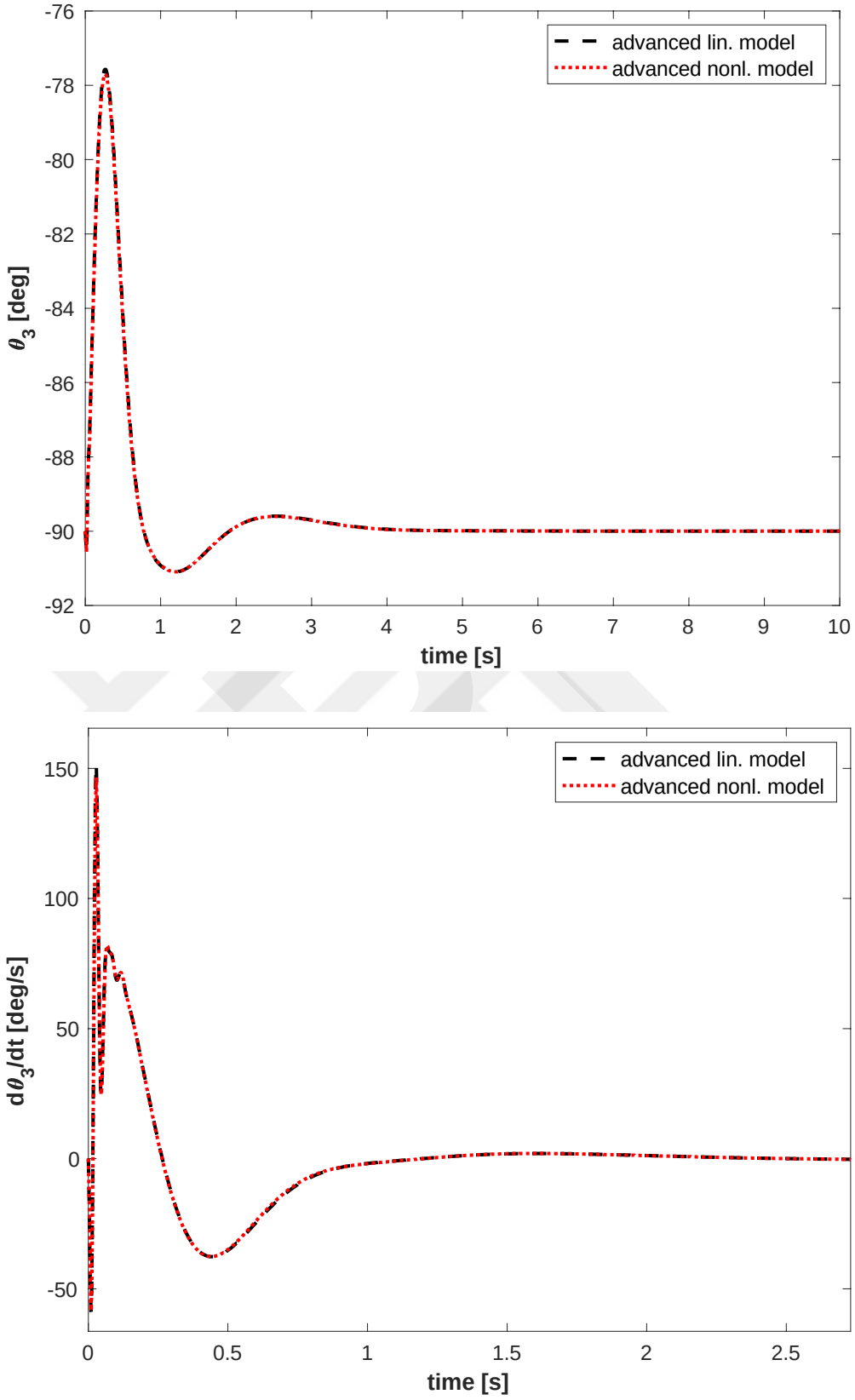

Figure 4.1 System Responses for the Hovering Condition.

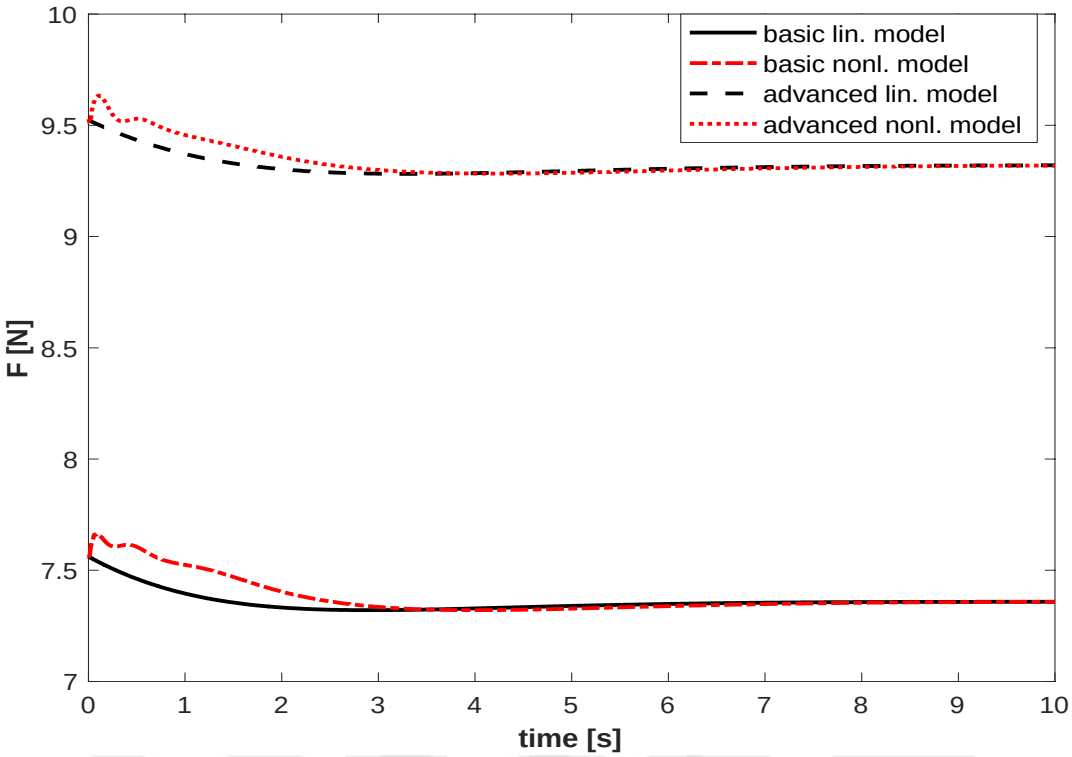
basic lin. model
basic nonl. model
advanced lin. model
advanced nonl. model
F [N]
time [s]
10
9.5
9
8.5
8
7.5
7
0
1
2
3
4
5
6
7
8
9
10

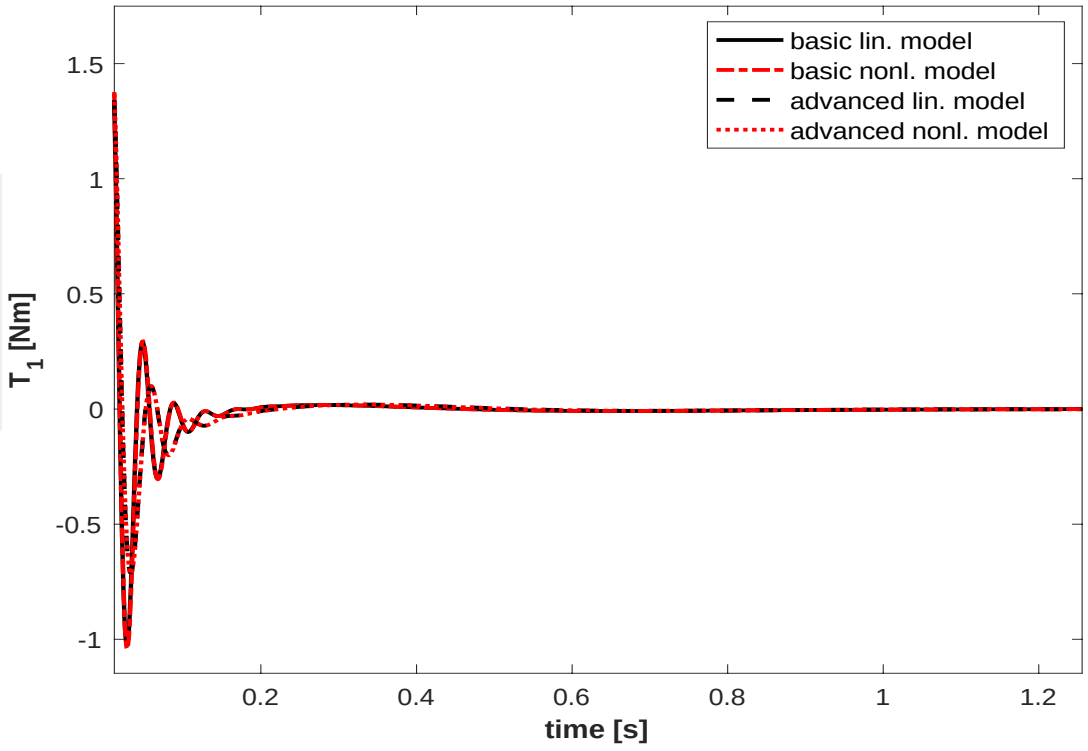
basic lin. model
basic nonl. model
advanced lin. model
advanced nonl. model
T 1 [Nm]
time [s]
1.5
1
0.5
0
-0.5
-1
0.2
0.4
0.6
0.8
1
1.2

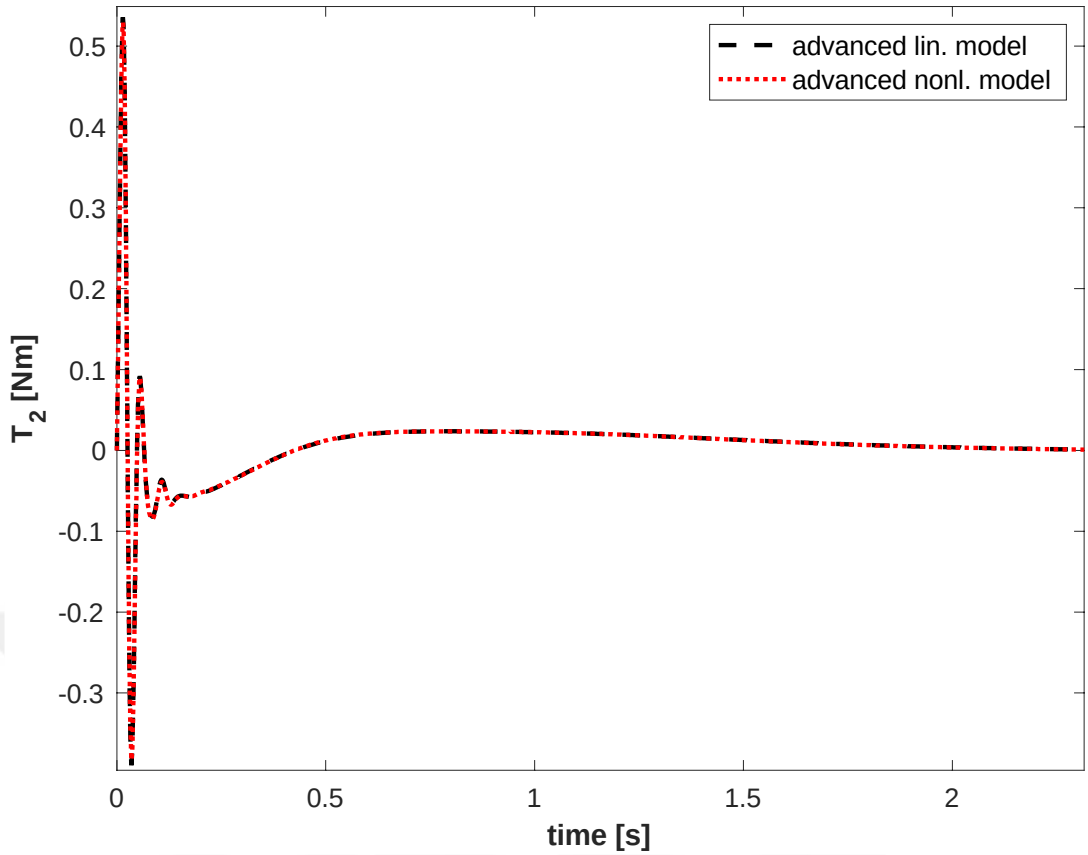

Figure 4.2. Control Inputs for the Hovering Condition.

The difference between the linear and nonlinear responses for the j^{th} state variable is presented using the function below. N is the total number of data points for the simulation. The first row of the table shows the error metric for the basic system and the second row presents the error metric for the advanced system.

$$S_j = \sum_i^N e_j^2(i), \tag{53}$$

where

$$e_j(i) = x_{j\_linear}(i) - x_{j\_nonlinear}(i) \tag{54}$$

Table 1. Sum of the square of errors between the linear and nonlinear models (First row: basic system; Second row: advanced system).

s_1	s_2	s_3	s_4	s_5	s_6	s_7	s_8	s_9	s_{10}
0.611	1.937	699.605	233.555	0.139	9.841	0.308	12.073		
0.220	0.491	350.3814	102.7750	0.0416	5.2779	0.1396	6.2448	0.0375	2.7910

4.2 SimulationsforNavigation

The nominal state vector used for the linearization of the basic system is given as follows.

$$x_{b\_nominal} = \left[0, 0, 0, 0, \frac{\pi}{2}, 0, -\frac{\pi}{2}, 0\right]^T$$

The nominal input vector for the linearization is given as below.

$$u_{b\_nominal} = [(m_1 + m_2)g, 0, 0, 0]^T$$

The following weighting matrices are used to design the LQR for the basic system.

$$Q_b = \text{diag}([1, 1, 2e\text{-}3, 2e\text{-}3, 1, 1, 0.15, 0.15, 100, 500]);$$

$$R_b = \text{diag}([1, 100])$$

The initial conditions for the state variables are given as below.

$$x_b(0) = \left[1, 0, 0.8, 0, \frac{40\pi}{180}, 0, 0, 0\right]^T$$

Analogously, the nominal state vector used for the linearization of the advanced system is given as follows.

$$\mathrm{x_{a\_nominal}} = \left[0, 0, 0, 0, \frac{\pi}{2}, 0, -\frac{\pi}{2}, 0, -\frac{\pi}{2}, 0\right]^{\mathrm{T}}$$

The nominal input vector for the linearization is

$$\mathrm{u_{a\_nominal}} = [(m_1 + m_2 + m_3)g, 0, 0, 0, 0]^{\mathrm{T}}$$

In order to compare with the response of the basic system, similar weighting matrices are used to design the controller for the advanced system.

$$Q_a = \mathrm{diag}([1, 1, 2\text{e-}3, 2\text{e-}3, 1, 1, 0.15, 0.15, 0.15, 0.15, 100, 500]);$$

$$R_a = \mathrm{diag}([1, 100, 100])$$

The initial conditions for the state variables are given as below.

$$\mathrm{x_a}(0) = \left[1, 0, 0.8, 0, \frac{40\pi}{180}, 0, 0, 0, 0, 0\right]^{\mathrm{T}}$$

Figure 4.3 presents the system responses and Figure 4.4 shows the control inputs for the basic and advanced systems.

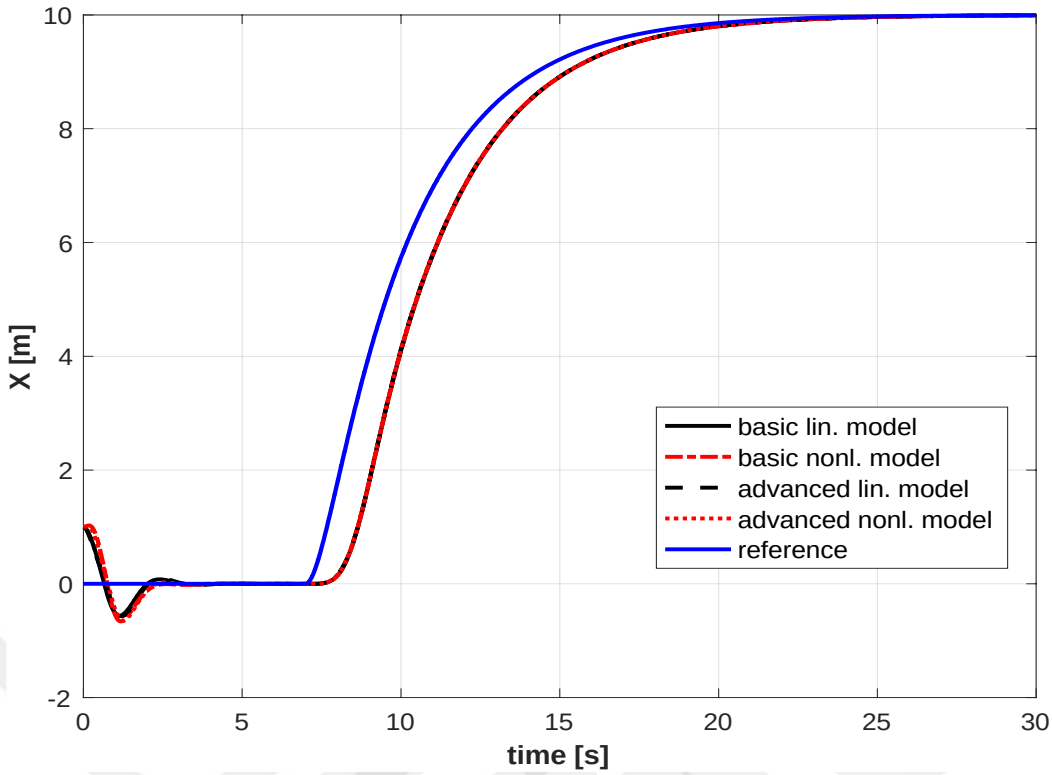
X [m]
time [s]
basic lin. model
basic nonl. model
advanced lin. model
advanced nonl. model
reference

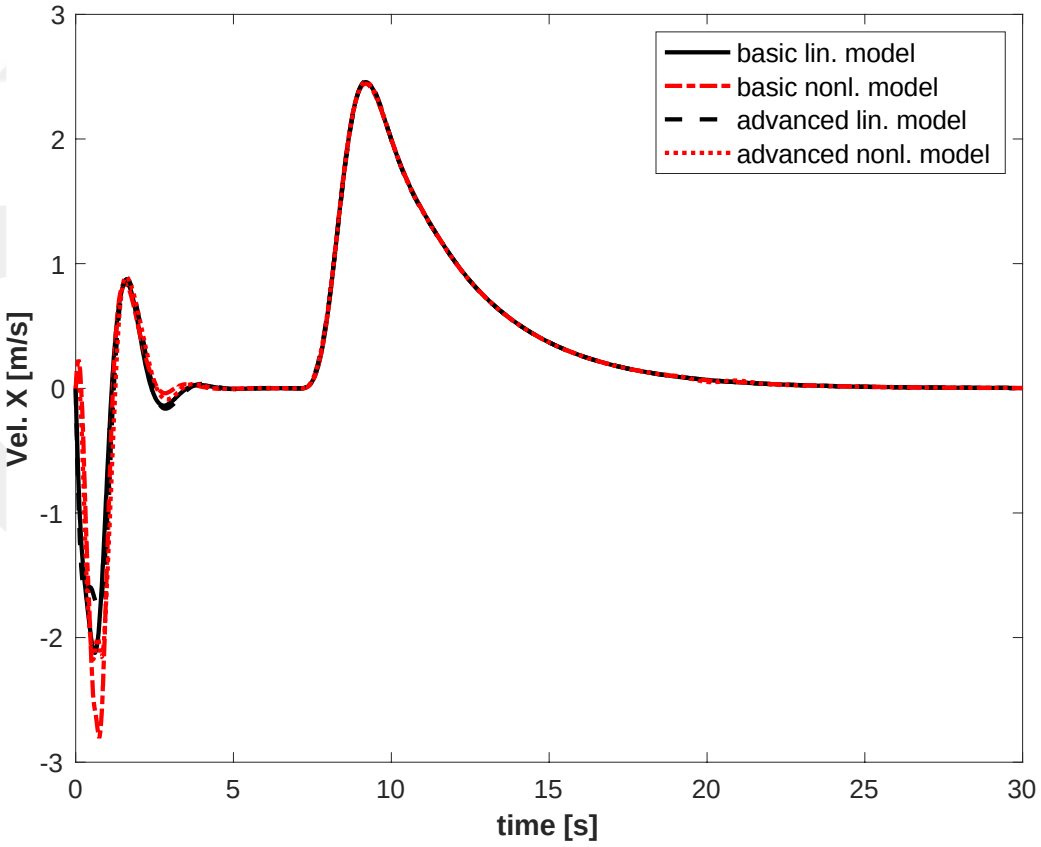
Vel. X [m/s]
time [s]
basic lin. model
basic nonl. model
advanced lin. model
advanced nonl. model

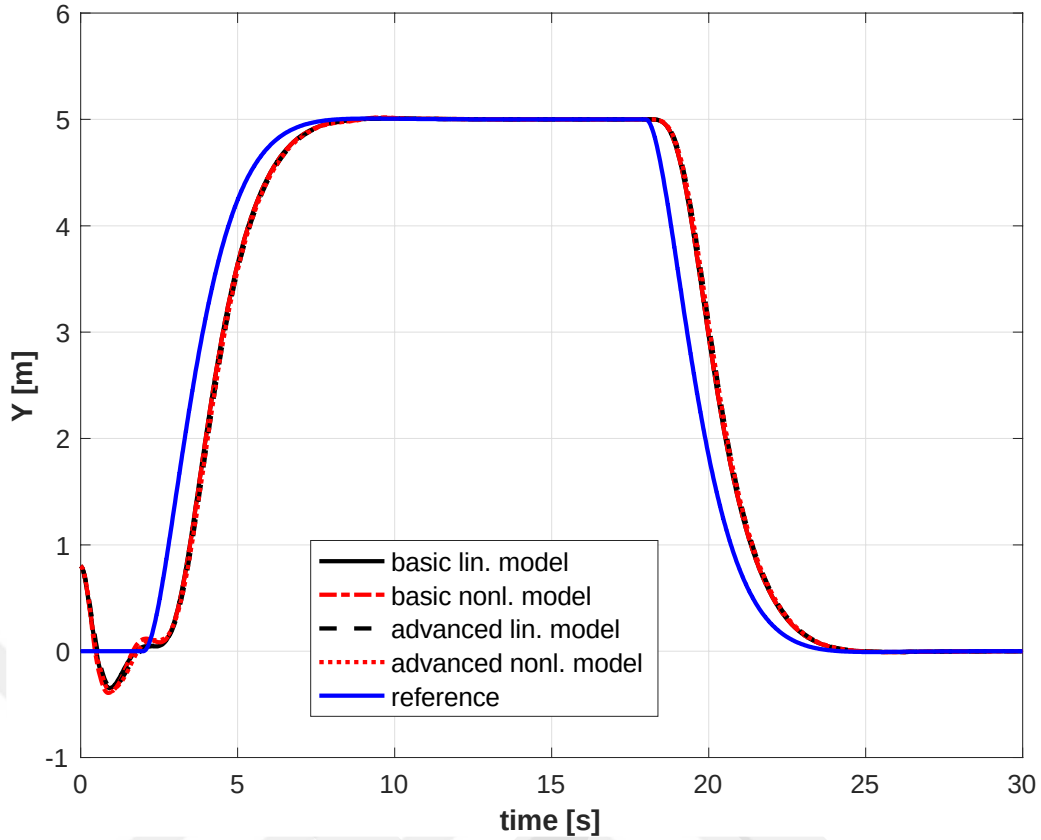
Y [m]
time [s]
basic lin. model
basic nonl. model
advanced lin. model
advanced nonl. model
reference

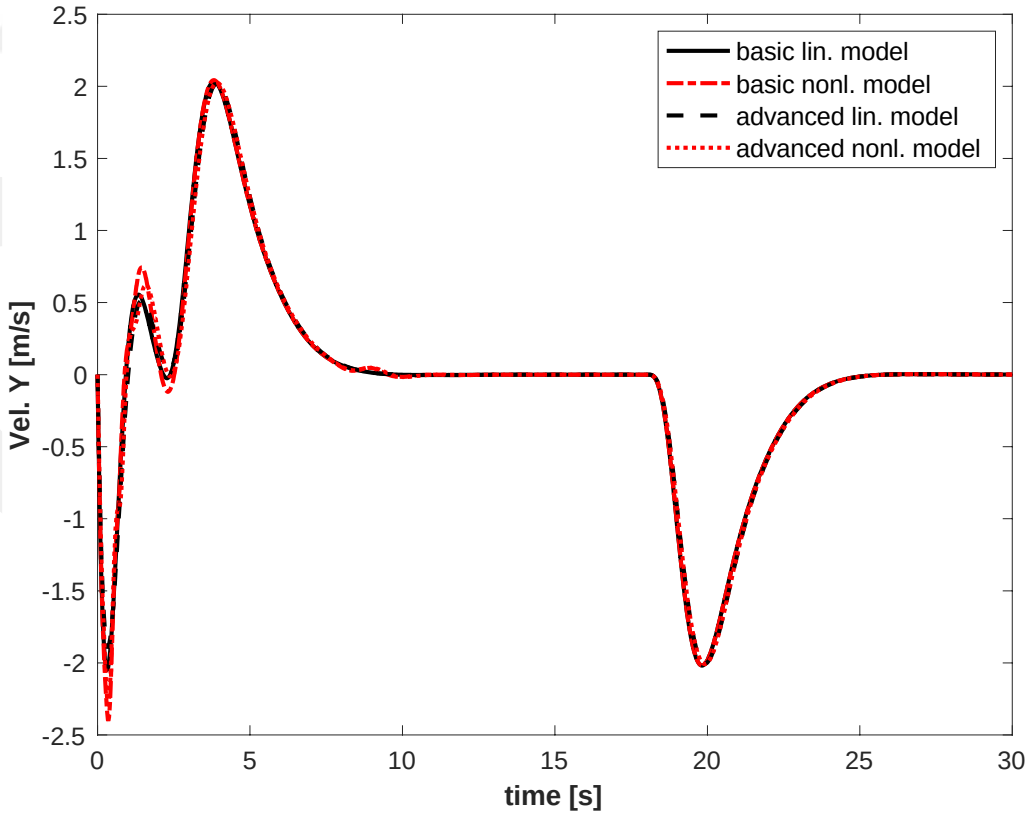
Vel. Y [m/s]
time [s]
basic lin. model
basic nonl. model
advanced lin. model
advanced nonl. model

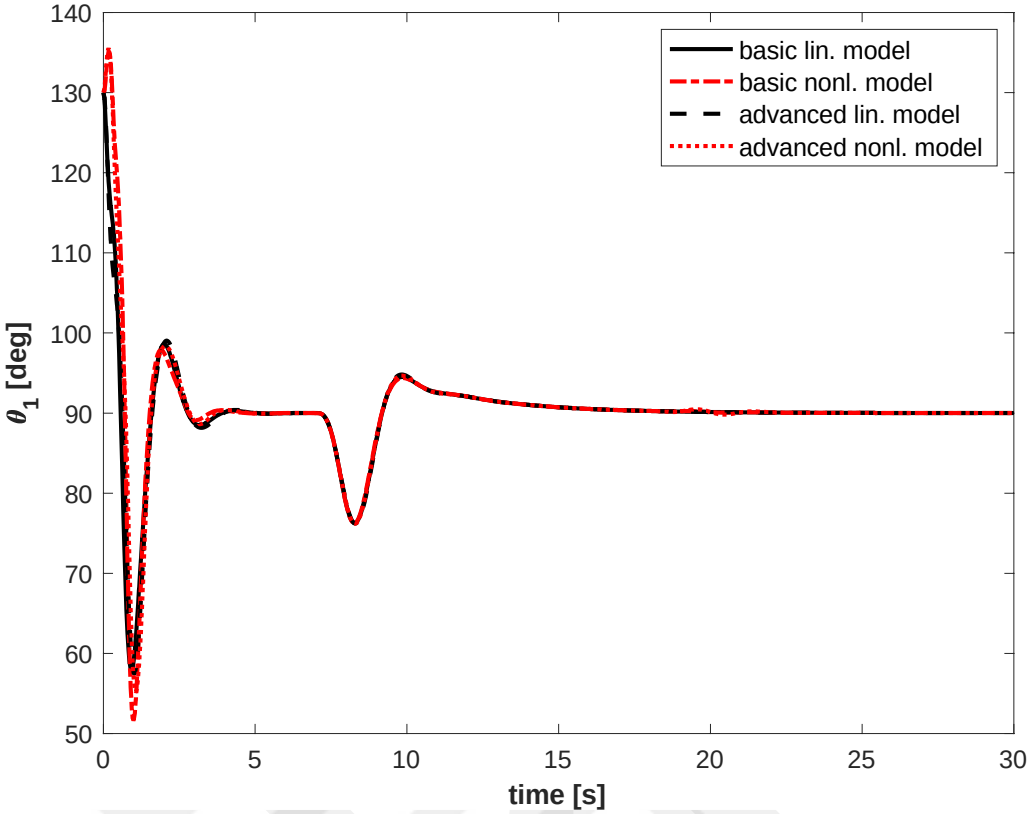
basic lin. model
basic nonl. model
advanced lin. model
advanced nonl. model
θ1 [deg]
time [s]

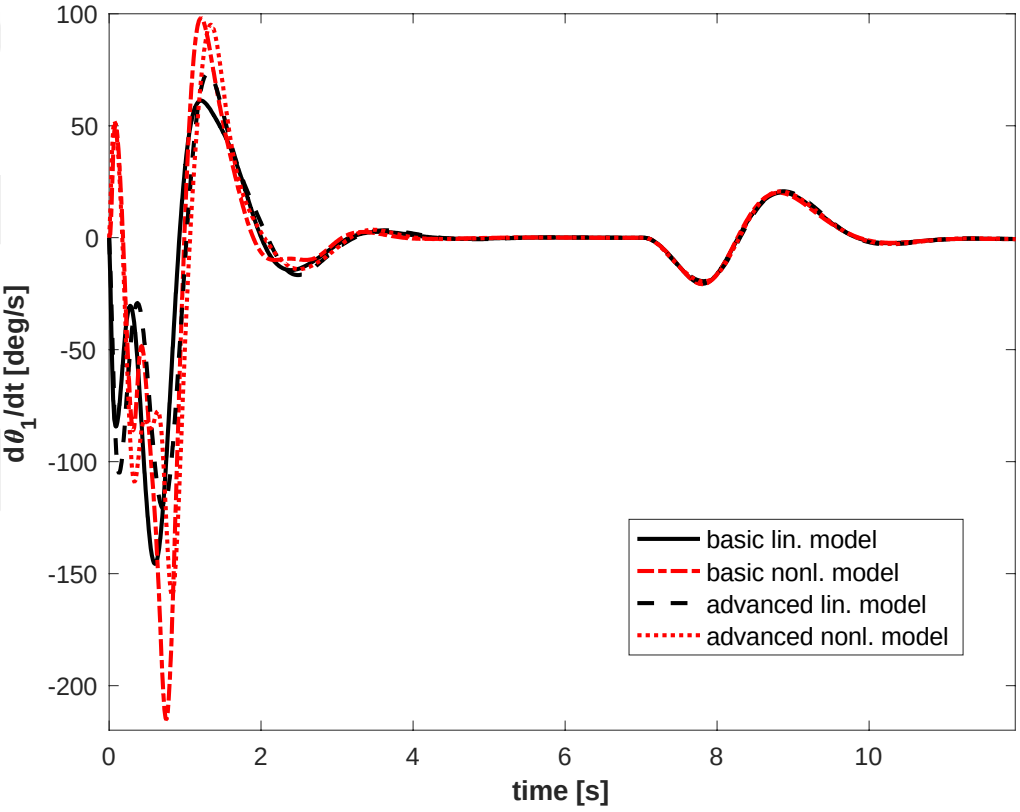
basic lin. model
basic nonl. model
advanced lin. model
advanced nonl. model
dθ1/dt [deg/s]
time [s]

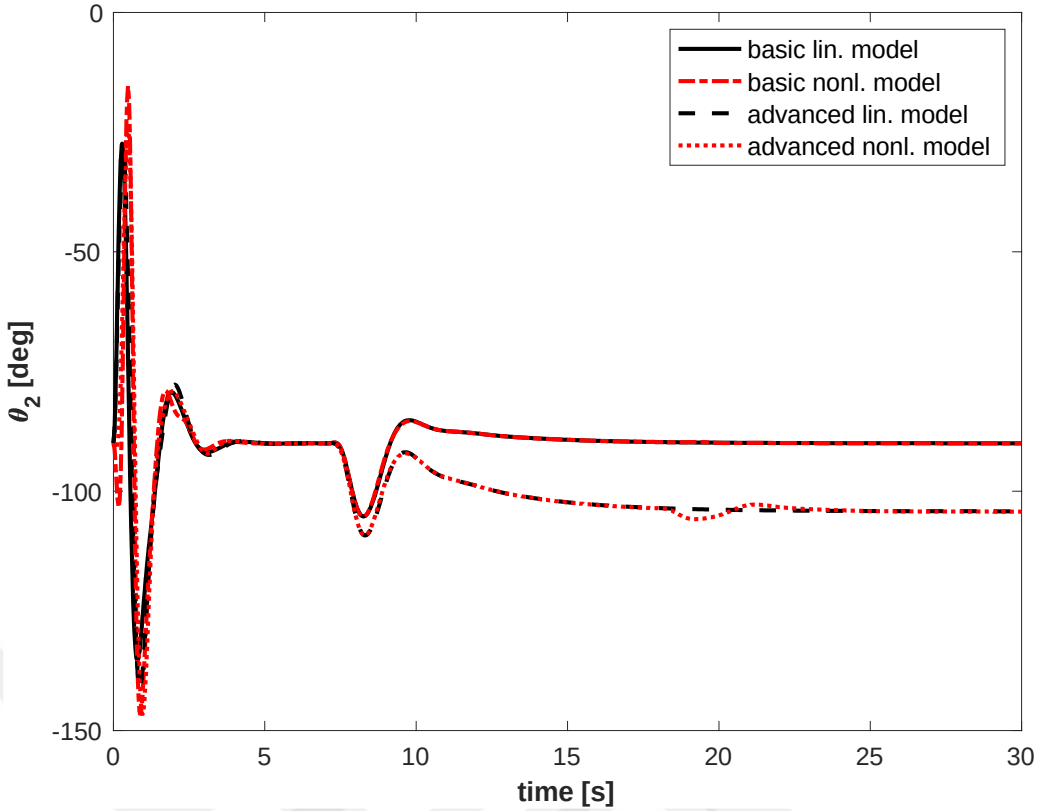
basic lin. model
basic nonl. model
advanced lin. model
advanced nonl. model
0
-50
-100
-150
θ2 [deg]
0
5
10
15
20
25
30
time [s]

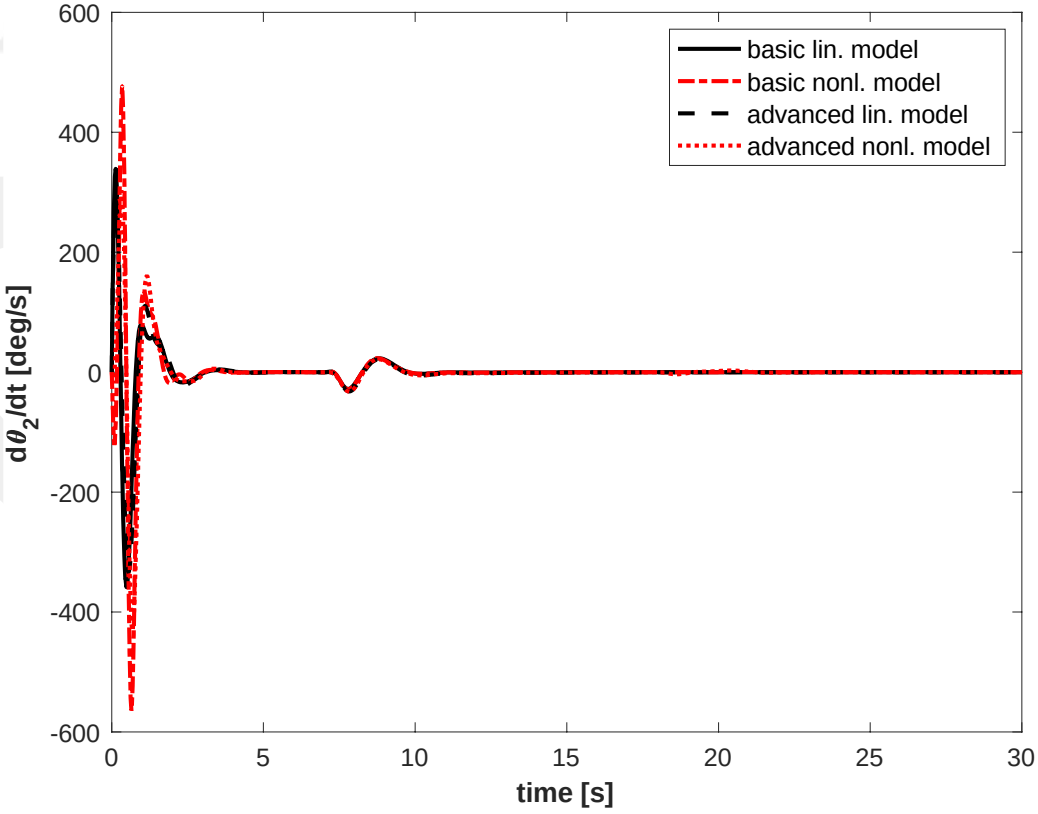
basic lin. model
basic nonl. model
advanced lin. model
advanced nonl. model
600
400
200
0
-200
-400
-600
dθ2/dt [deg/s]
0
5
10
15
20
25
30
time [s]

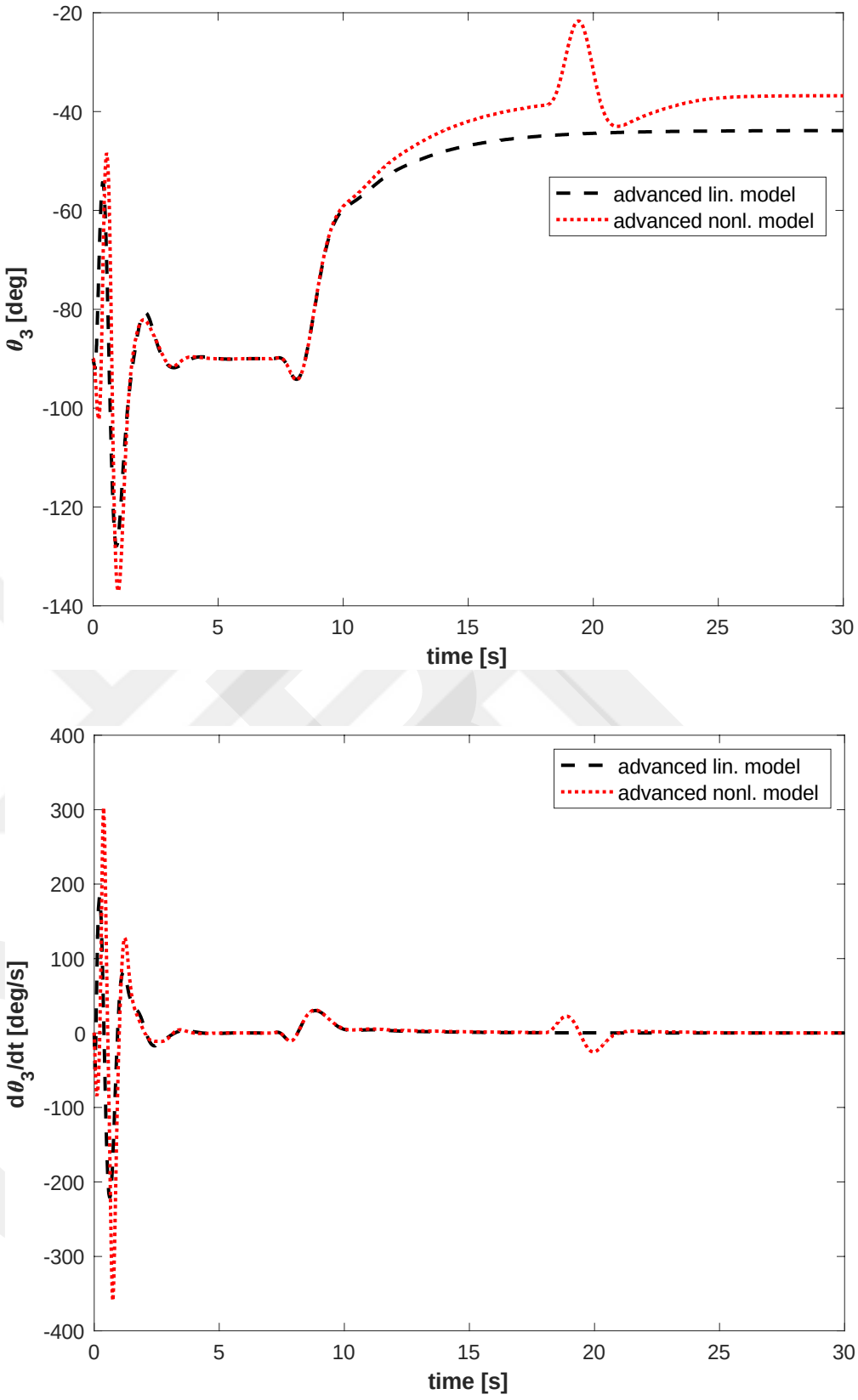

Figure 4.3 System Responses during Navigation.

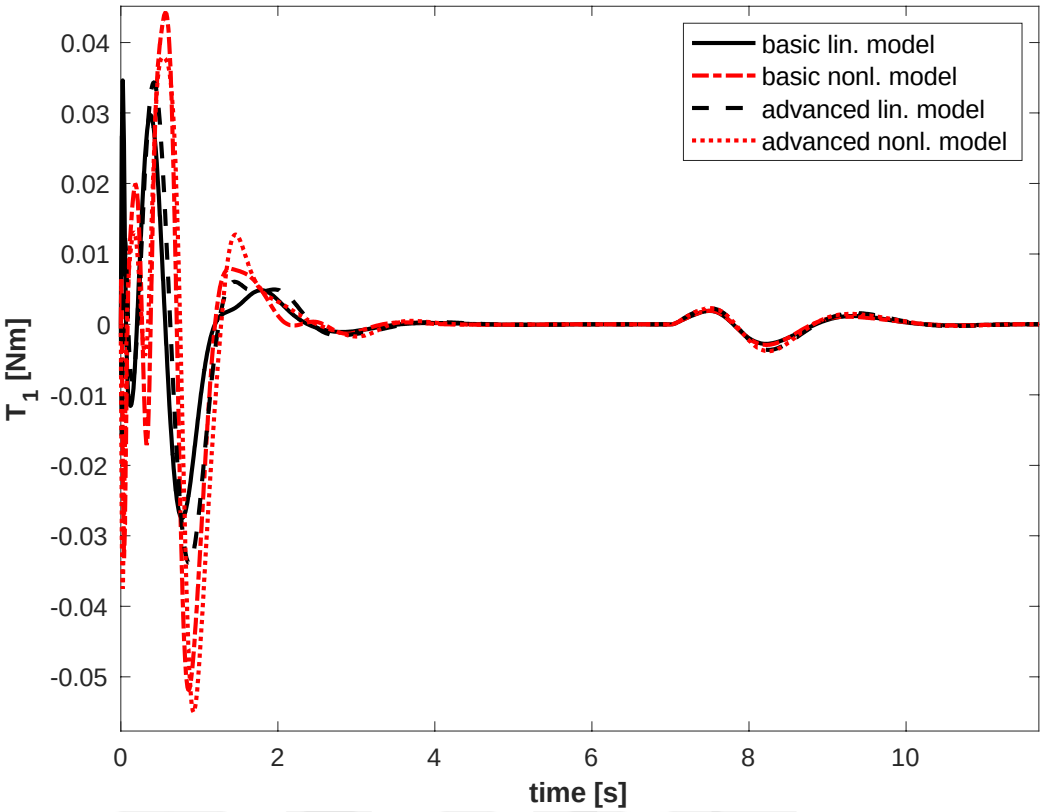
basic lin. model
basic nonl. model
advanced lin. model
advanced nonl. model
T 1 [Nm]
time [s]

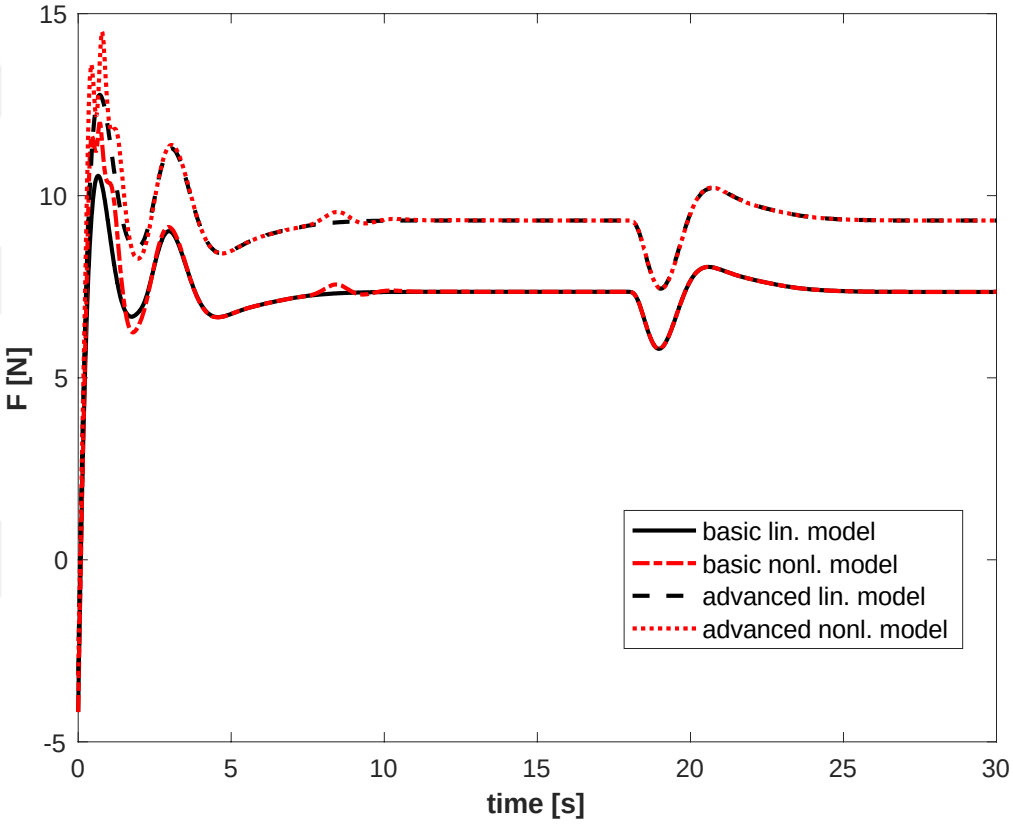
basic lin. model
basic nonl. model
advanced lin. model
advanced nonl. model
F [N]
time [s]

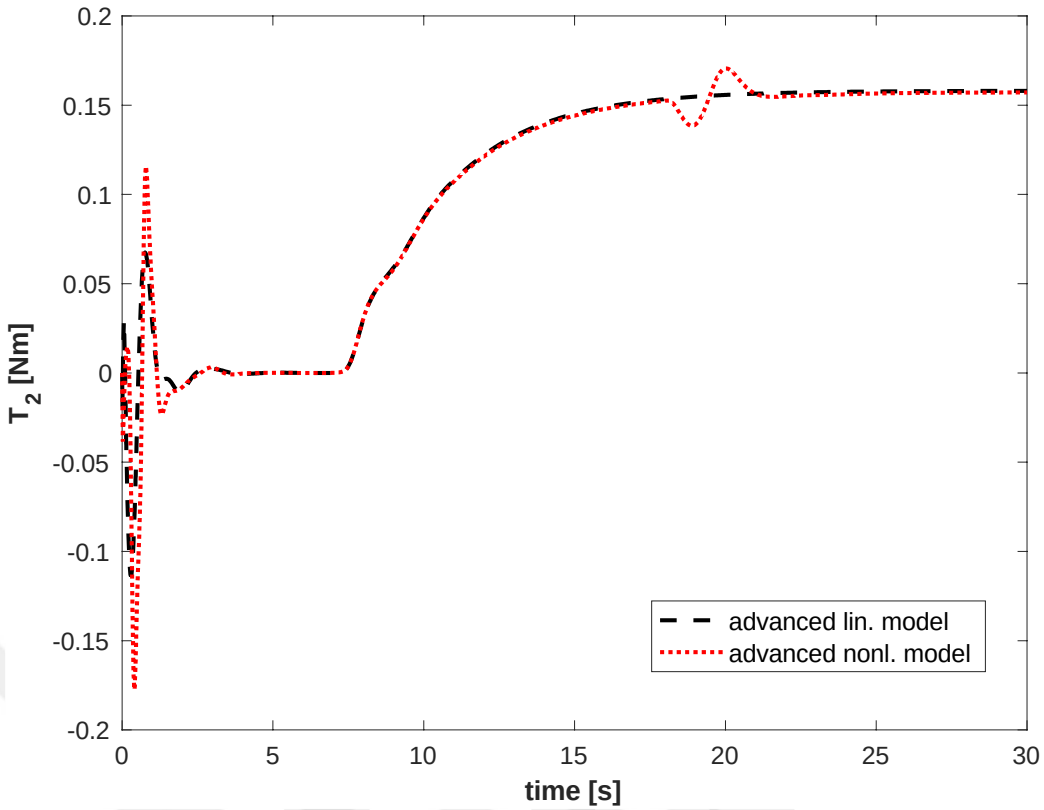

Figure 4.4 Control Inputs for Navigation

The performances of the basic and advanced systems are compared as the external inputs F_{ex} and F_{ey} are applied. The corresponding weighting matrices are given as below.

$$Q_b = \text{diag}([1, 1, 2e\text{-}3, 2e\text{-}3, 1, 1, 0.15, 0.15, 100, 500]),$$

$$R_b = \text{diag}([1, 100])$$

$$Q_a = \text{diag}([1, 1, 2e\text{-}3, 2e\text{-}3, 1, 1, 0.15, 0.15, 0.15, 0.15, 100, 500])$$

$$R_a = \text{diag}([1, 100, 100])$$

The forces used in the simulations are given as below.

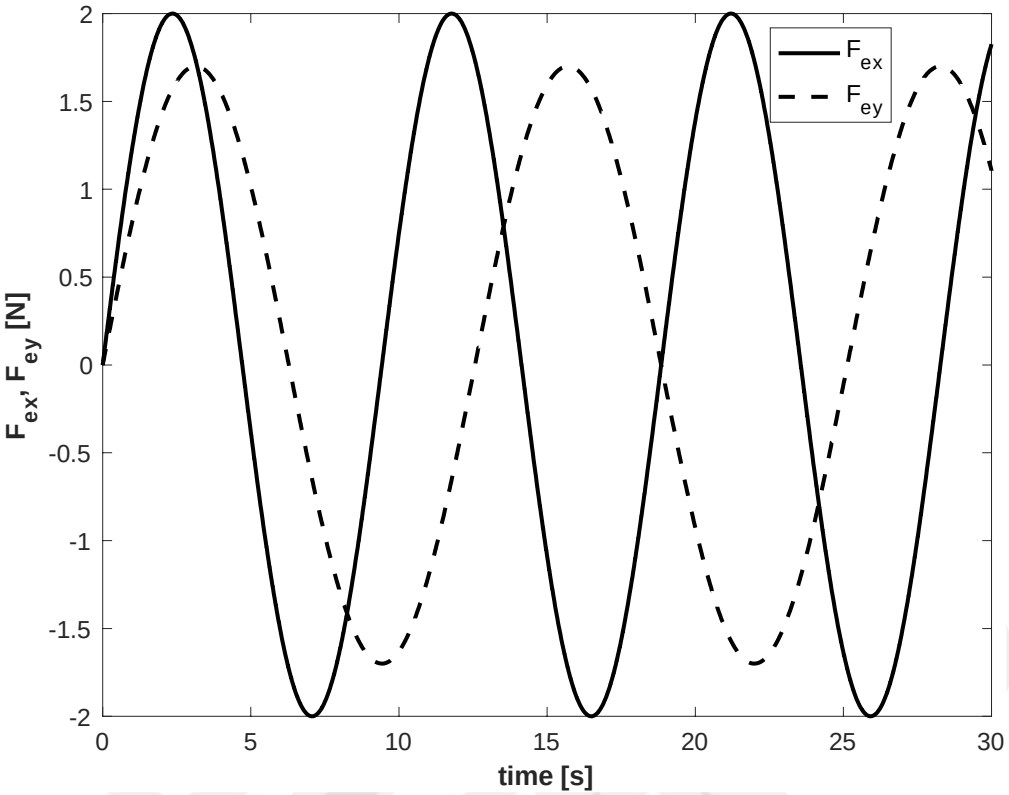

Figure 4.5 External Forces

Figure 4.6 presents the system responses and Figure 4.7 shows the control inputs for the basic and advanced systems.

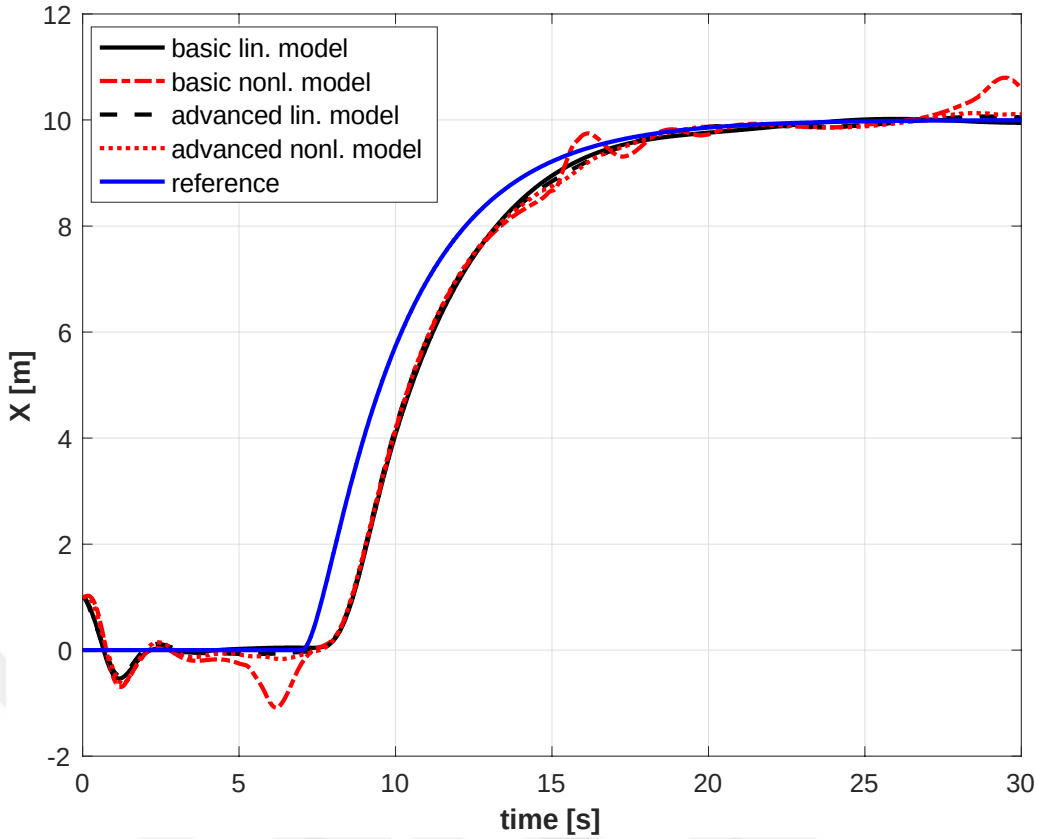
basic lin. model
basic nonl. model
advanced lin. model
advanced nonl. model
reference
X [m]
time [s]

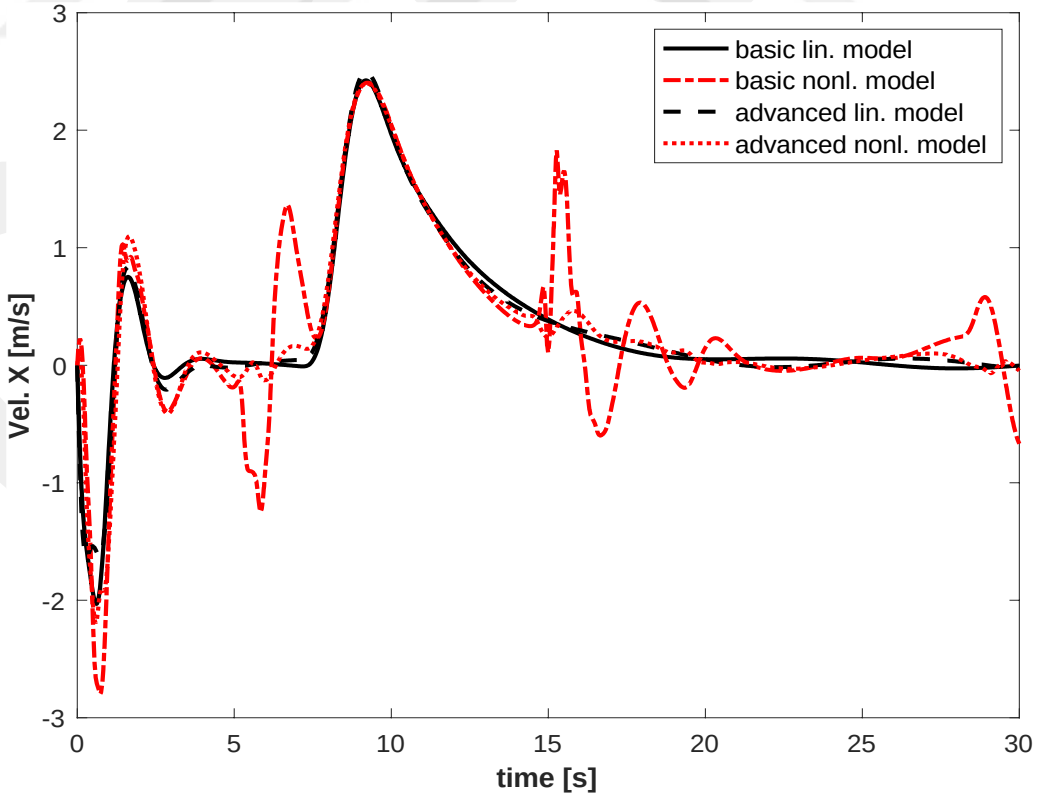
basic lin. model
basic nonl. model
advanced lin. model
advanced nonl. model
Vel. X [m/s]
time [s]

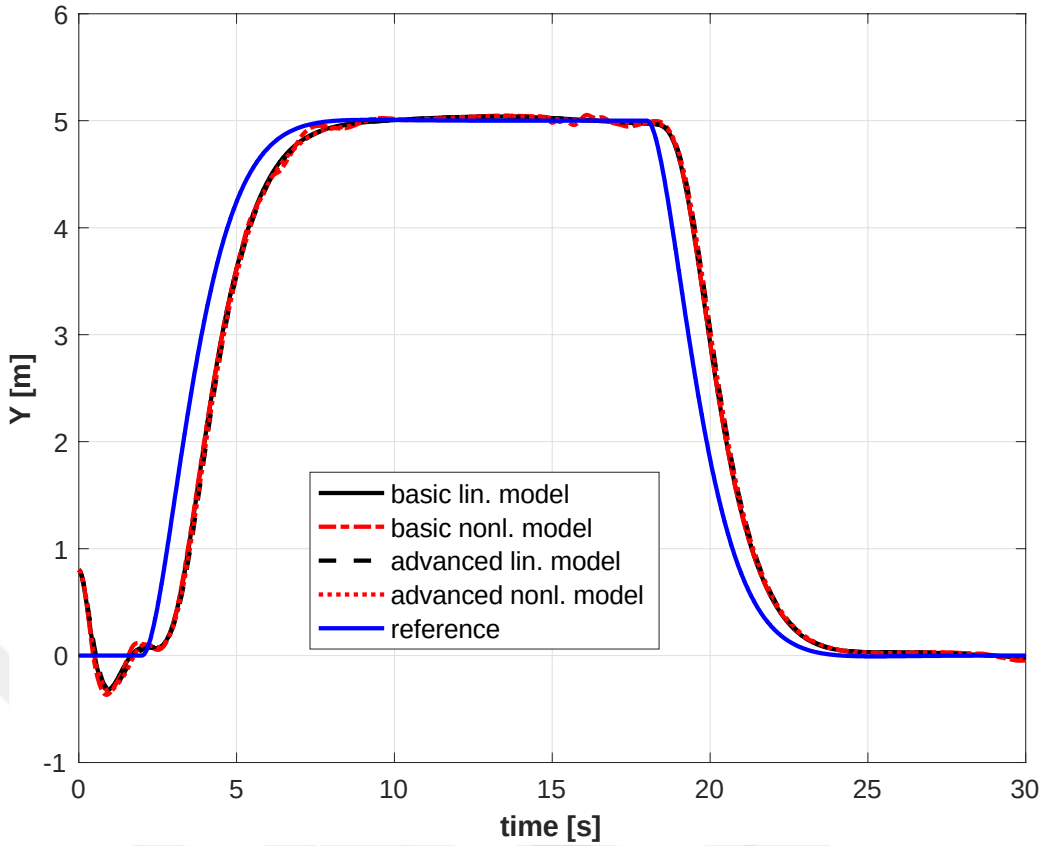
Y [m]
time [s]
basic lin. model
basic nonl. model
advanced lin. model
advanced nonl. model
reference

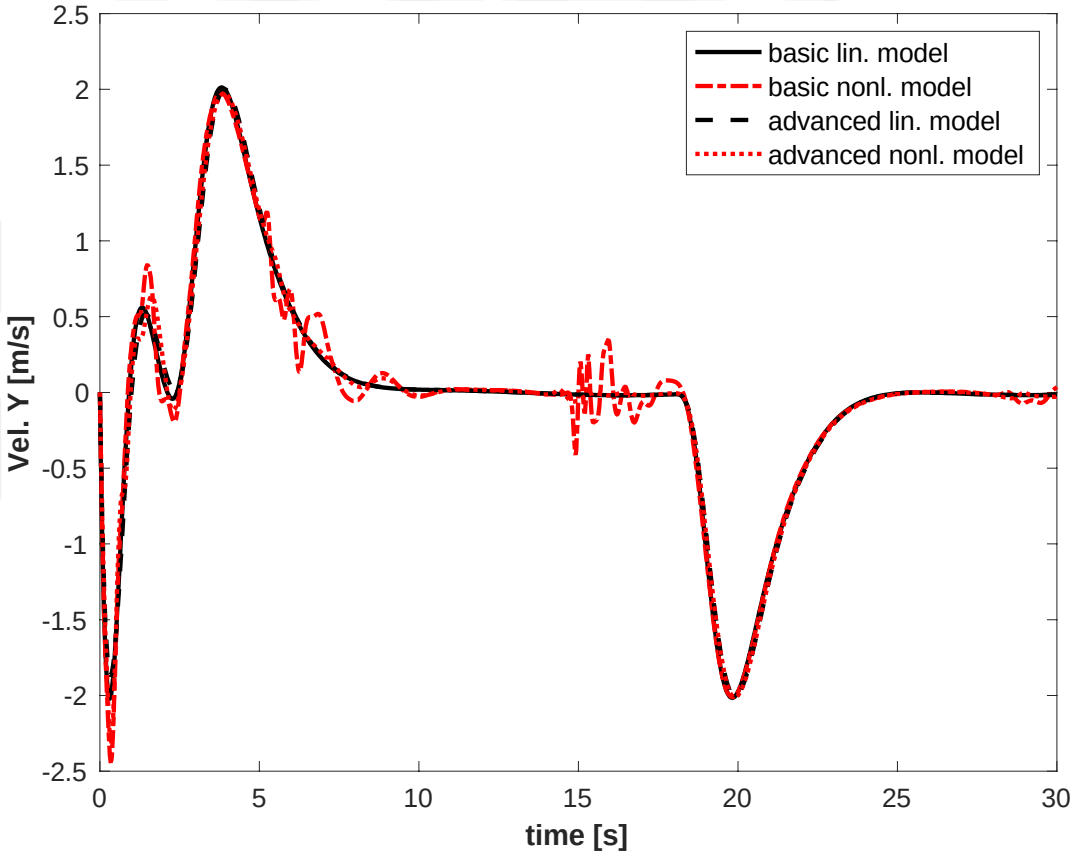
Vel. Y [m/s]
time [s]
basic lin. model
basic nonl. model
advanced lin. model
advanced nonl. model

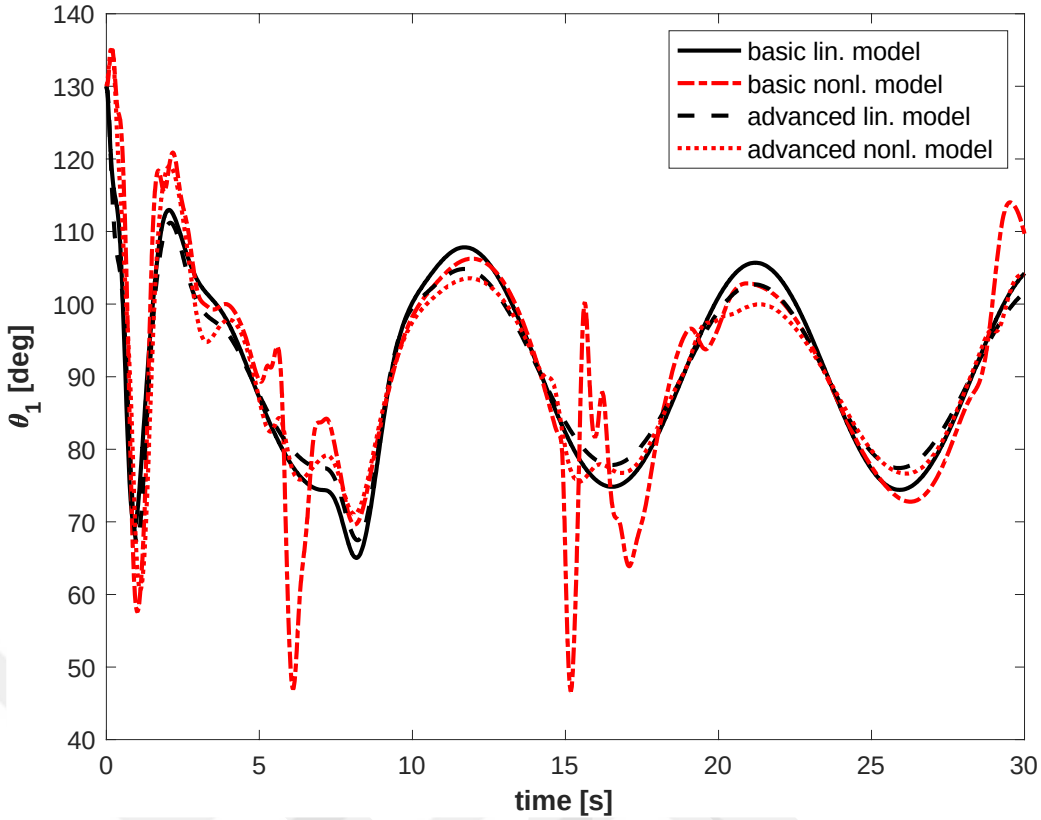
basic lin. model
basic nonl. model
advanced lin. model
advanced nonl. model
θ_1 [deg]
time [s]

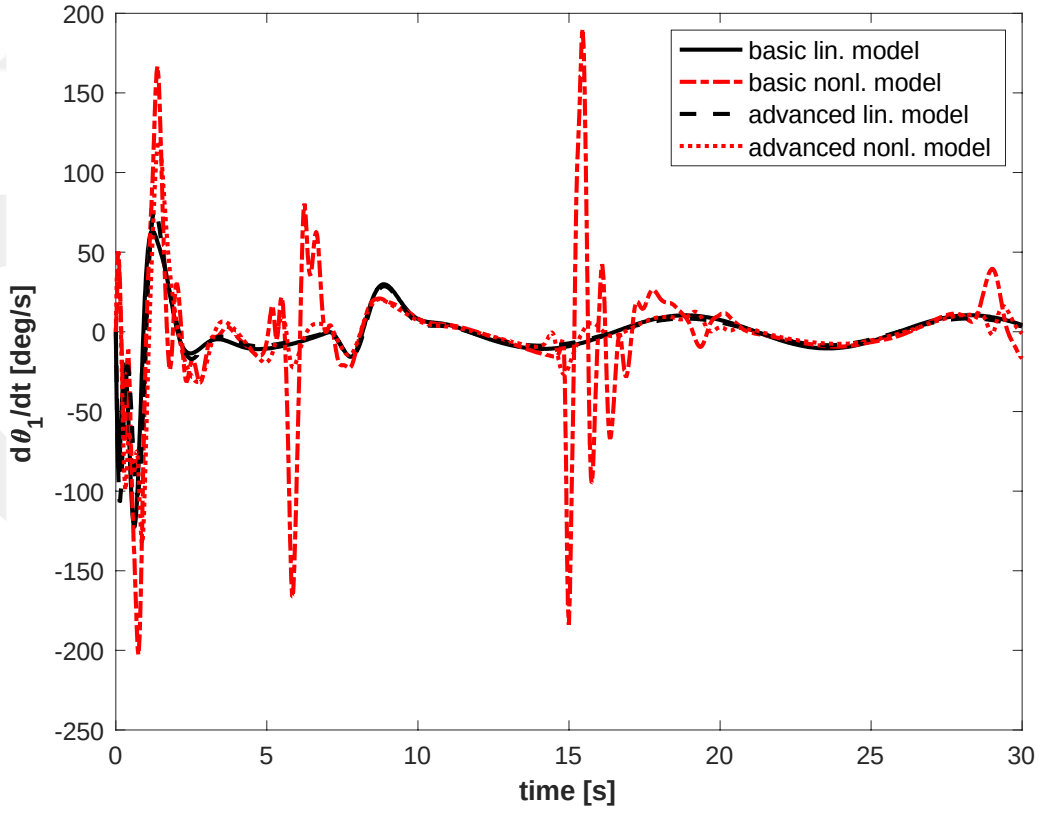
basic lin. model
basic nonl. model
advanced lin. model
advanced nonl. model
$d\theta_1/dt$ [deg/s]
time [s]

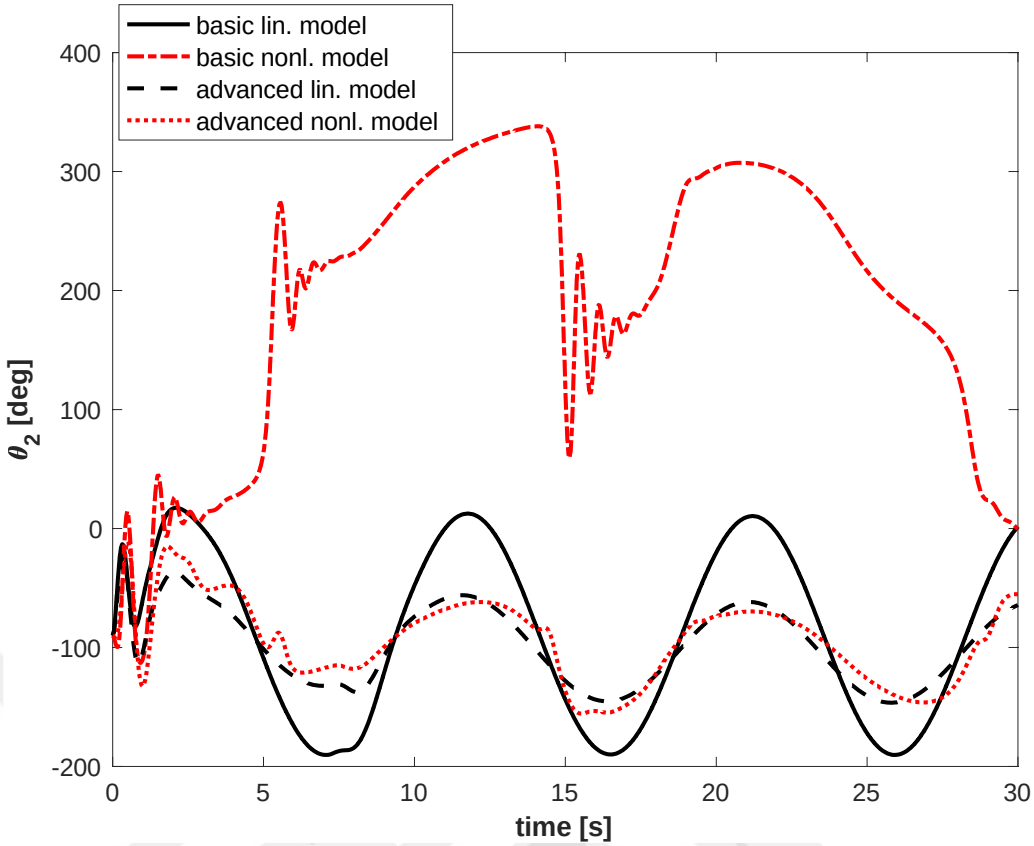
basic lin. model
basic nonl. model
advanced lin. model
advanced nonl. model
400
300
200
100
0
-100
-200
θ2 [deg]
0
5
10
15
20
25
30
time [s]

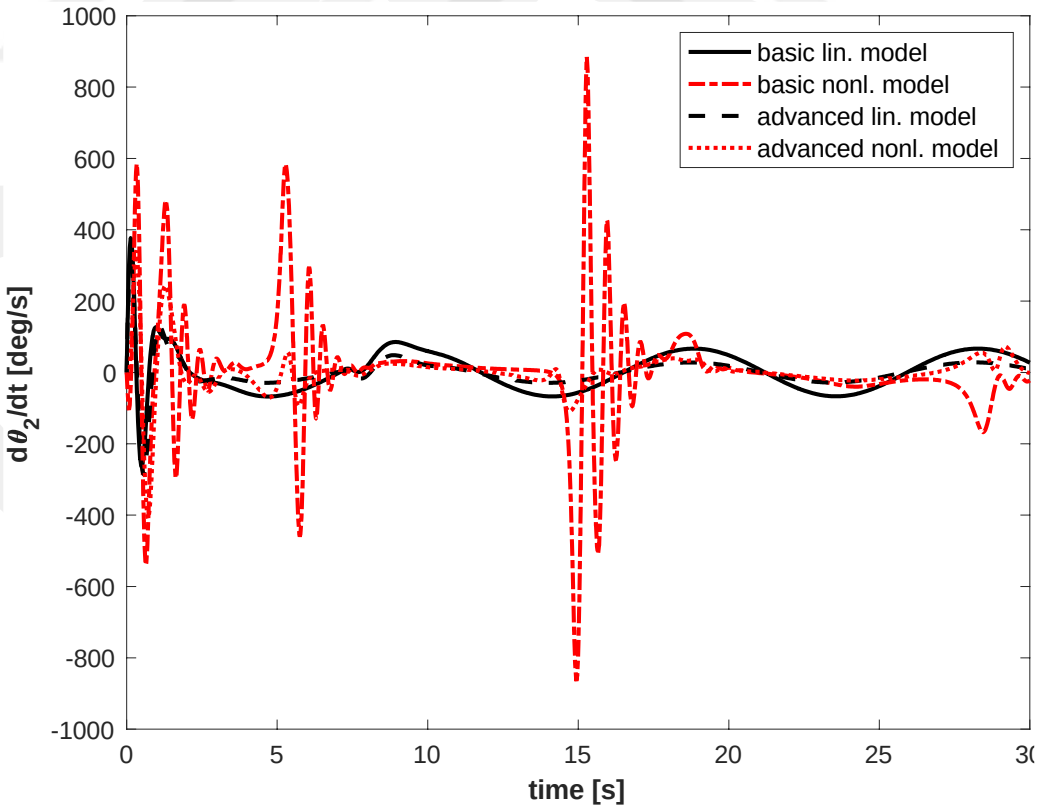
basic lin. model
basic nonl. model
advanced lin. model
advanced nonl. model
1000
800
600
400
200
0
-200
-400
-600
-800
-1000
dθ2/dt [deg/s]
0
5
10
15
20
25
30
time [s]

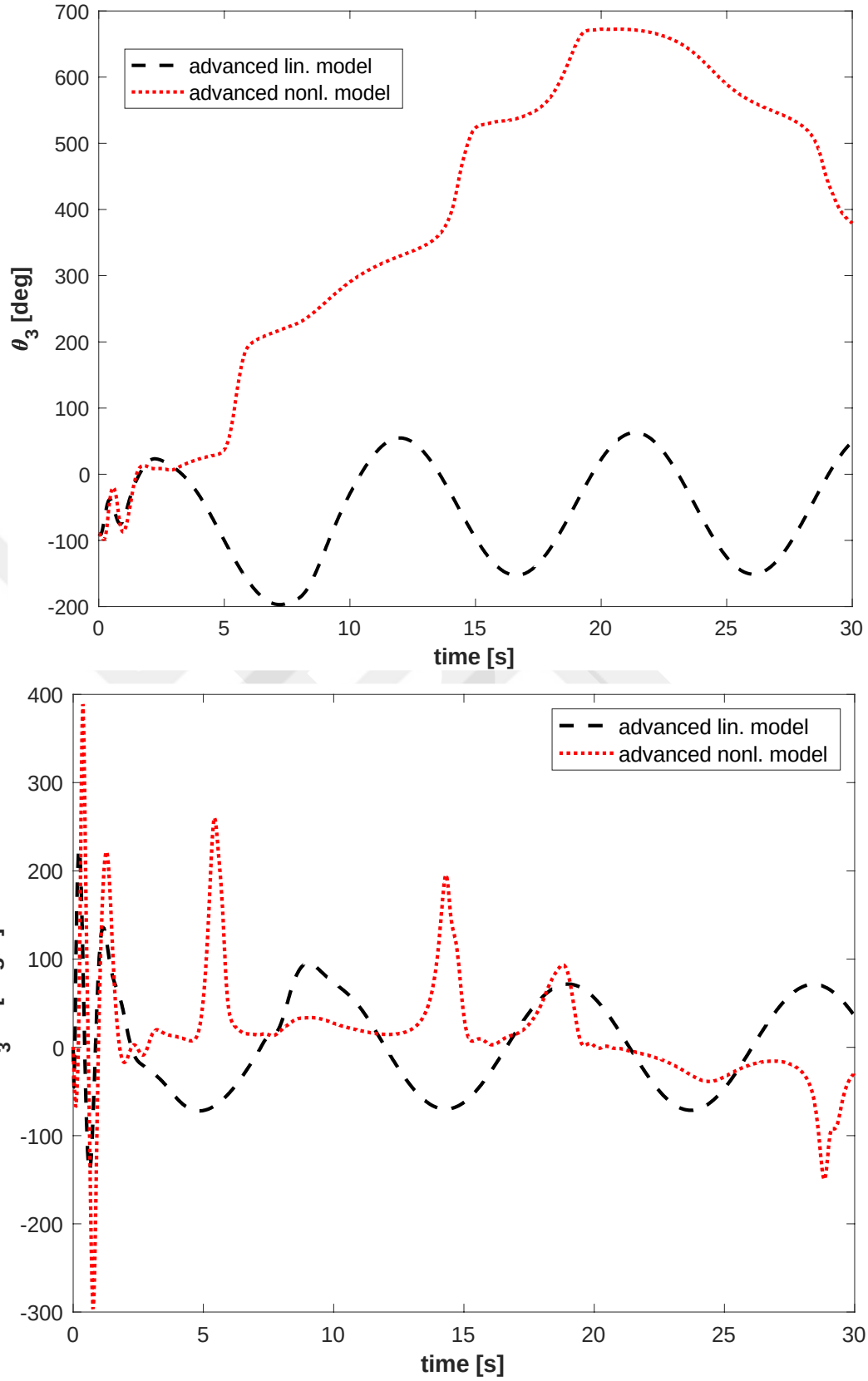

Figure 4.6 System Responses during Navigation as External Forces Acting

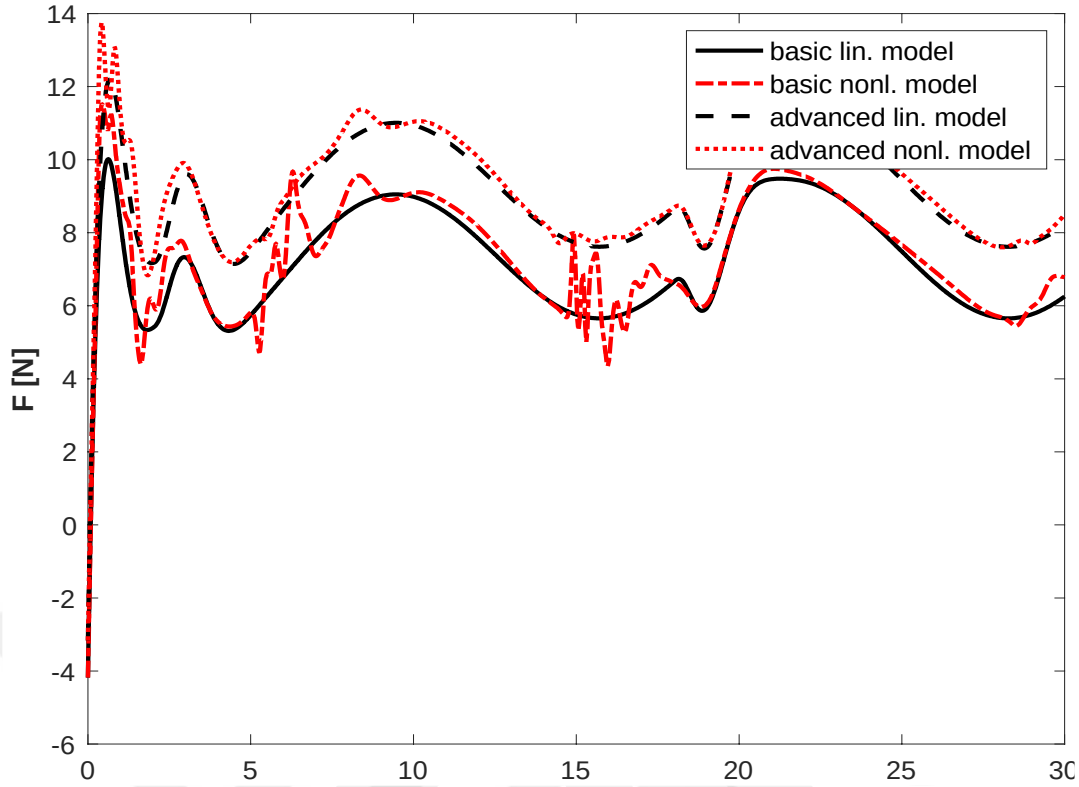
basic lin. model
basic nonl. model
advanced lin. model
advanced nonl. model
F [N]
14
12
10
8
6
4
2
0
-2
-4
-6
0
5
10
15
20
25
30

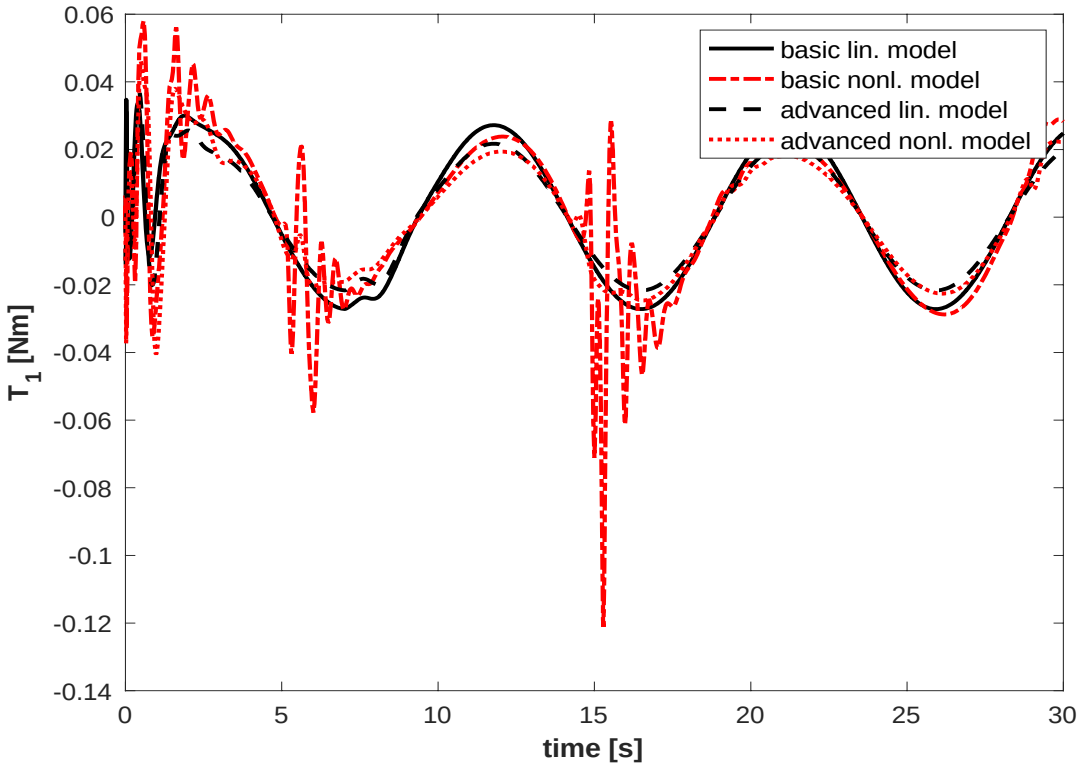
basic lin. model
basic nonl. model
advanced lin. model
advanced nonl. model
T1 [Nm]
0.06
0.04
0.02
0
-0.02
-0.04
-0.06
-0.08
-0.1
-0.12
-0.14
0
5
10
15
20
25
30
time [s]

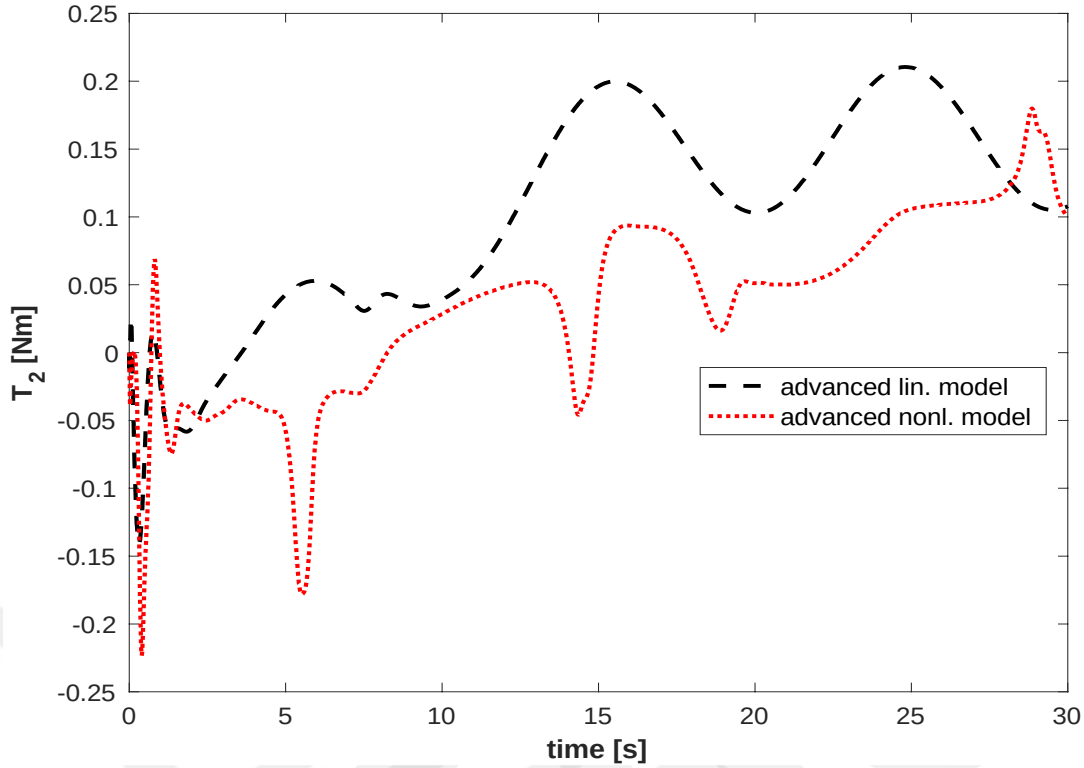

Figure 4.7 Control Inputs for Navigation as External Forces Acting

The utilized weighting matrices provide robust tracking performance. The tracking performance is quantified by using the tracking error, as well.

$$S_{k\_m}^{t} = \sum_{i}^{N} e_{k\_m}^{2}(i) \tag{55}$$

where

$$e_{k\_m}(i) = R_k(i) - y_{k_m}(i)$$

$$t = \{bs, ad\}, k = \{1, 2\}, m = \{linear, nonlinear\}$$

Table 2. Sum of the square of the tracking errors normalized values.

$s_{1\_linear\_}^{bs}$	$s_{1\_nonlinear\_}^{bs}$	$s_{2\_linear\_}^{bs}$	$s_{2\_nonlinear\_}^{bs}$	$s_{1\_linear\_}^{ad}$	$s_{1\_nonlinear\_}^{ad}$	$s_{2\_linear\_}^{ad}$	$s_{2\_nonlinear\_}^{ad}$
1.3783	1.5473	0.5755	0.5754	1.2861	1.3138	0.6697	0.6646

4.3 Simulations for Navigation with Admittance Control

Following external forces are applied so as to test the robustness of the basic and advanced systems as the navigation control presented in the previous section is employed.

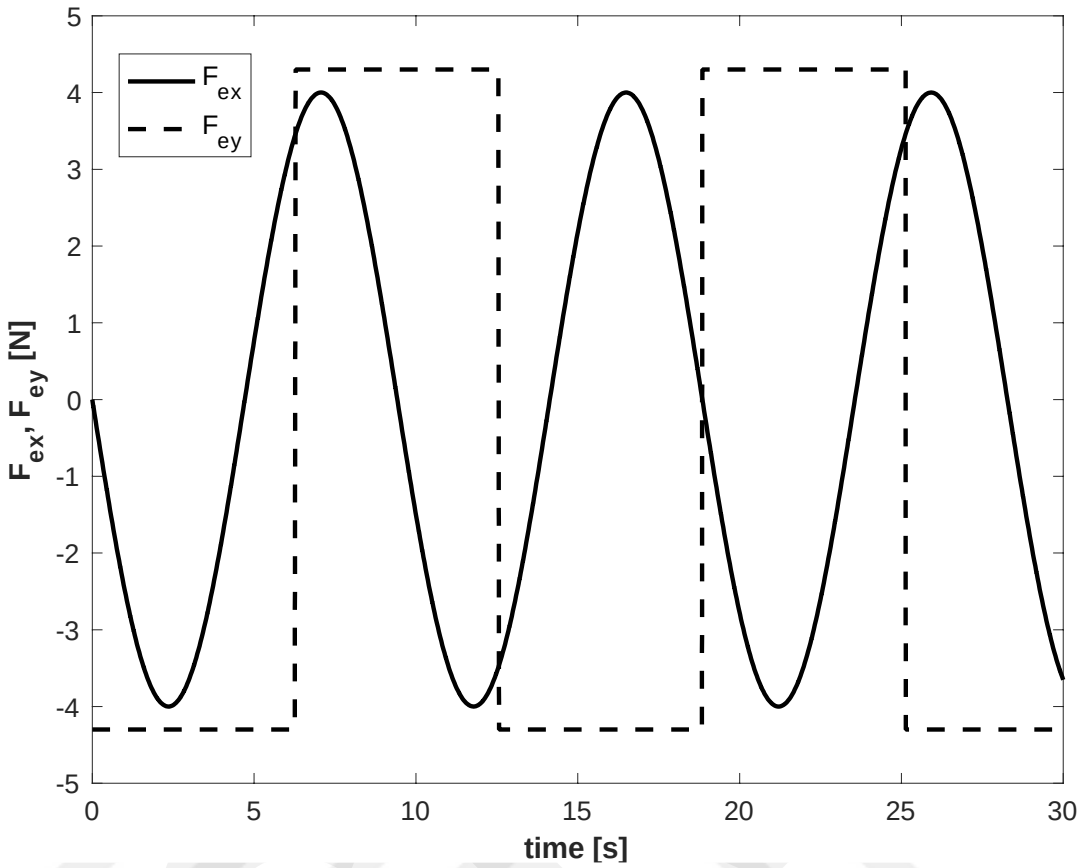

Figure 4.8 Compelling-External Forces

While the linear model for the basic system seems to reject the disturbances in Figure 4.9 the nonlinear response unveils an unstable behavior.

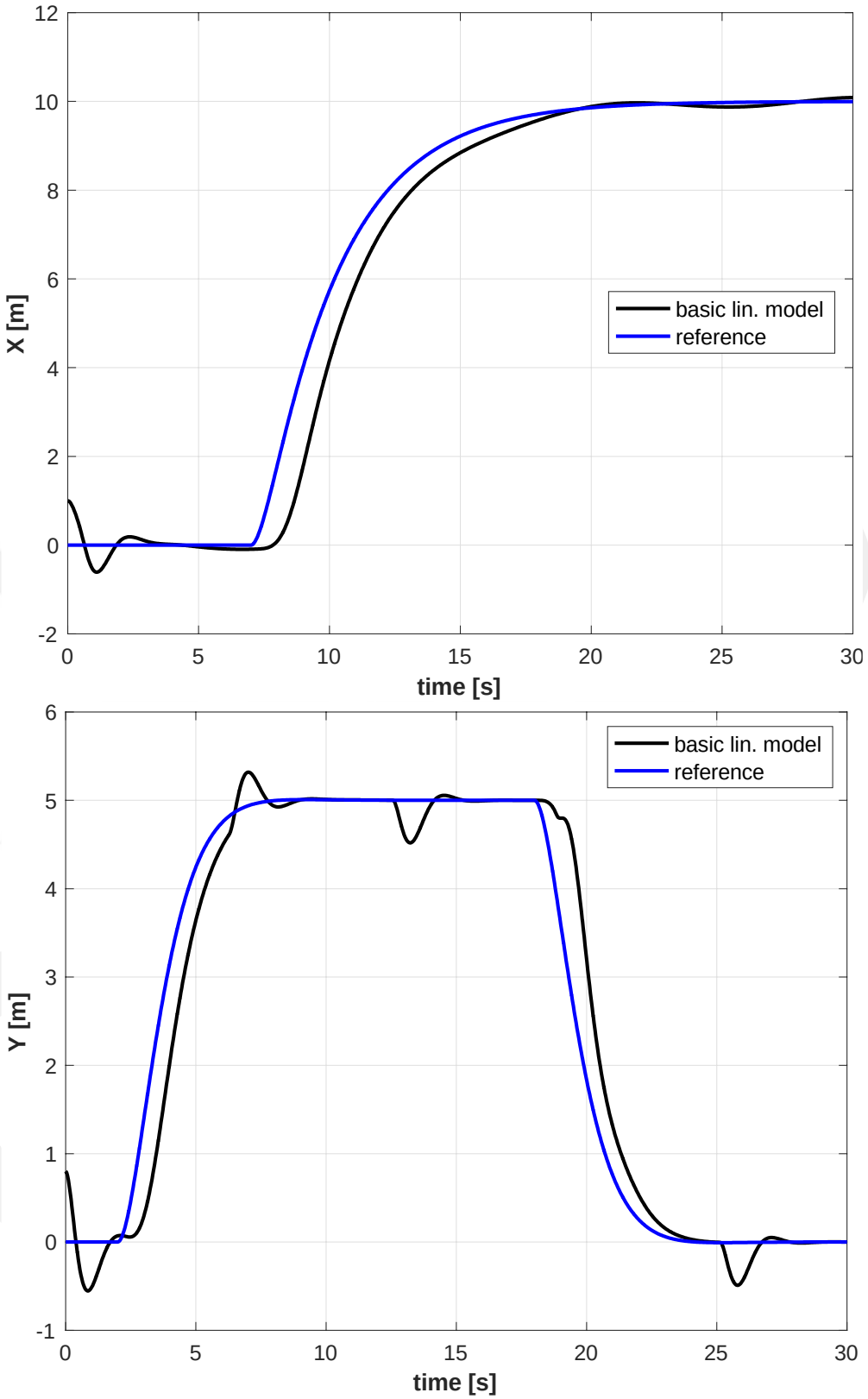

Figure 4.9 Response of the Linear Model for the Basic System due to the External Forces in Figure 4.8

On the other hand, the advanced system has the potential to reject the effects of the external forces in Figure 4.8 As presented in Figure 4.10, both the linear and nonlinear responses of the advanced system unveil stable behavior.

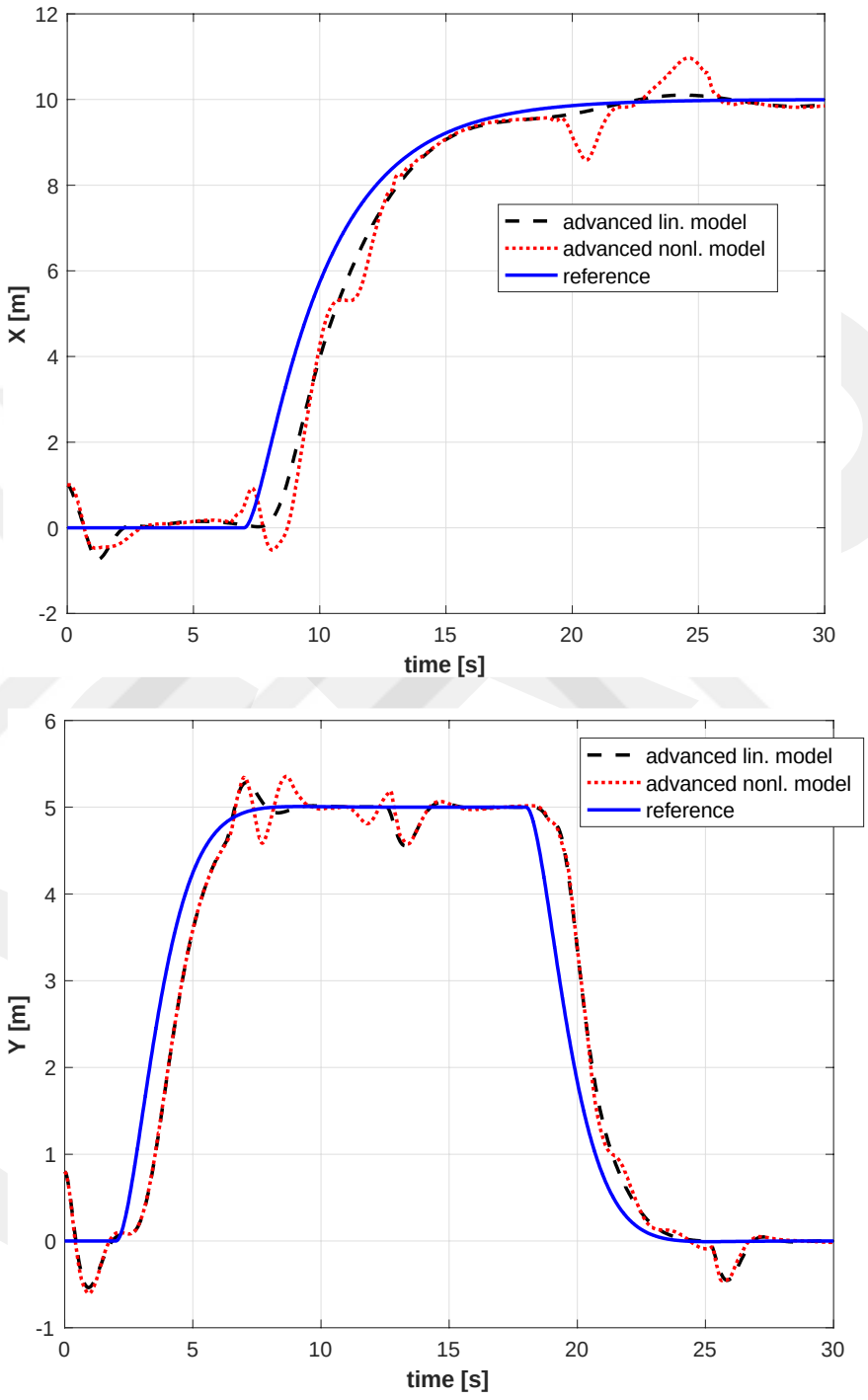

Figure 4.10. Response of the Advanced System due to the External Forces in Figure 4.8

Once the admittance control is applied to modify the reference inputs, the basic system withstands the external forces and performs a stable navigation (Figure 4.11).

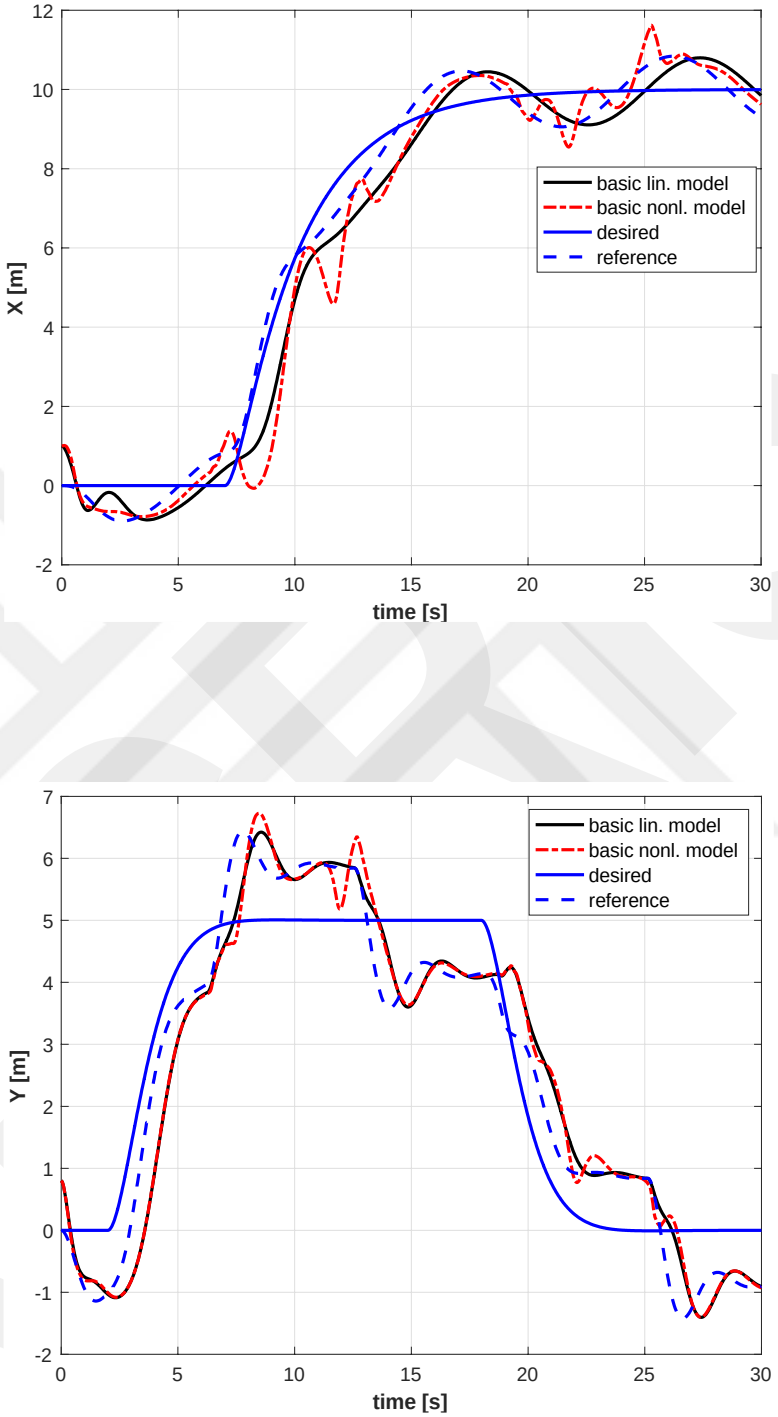

Figure 4.11 Response of the Admittance Controlled Basic System due to the External Forces in Figure 4.8

CHAPTER 5

DISCUSSION

Considering linear and nonlinear simulations of the basic and advanced systems for hovering, it is seen that the behaviors are similar in terms of the linear and nonlinear responses except the altitude state, Y, and the corresponding velocity, $\dot{Y}$. As seen in Table 1, the differences between the linear and nonlinear responses for the basic and advanced systems show the highest amplitude for these two state variables. This result agrees with the minimum singular values of the basic and advanced system showing the direction, which is difficult to be controlled. The comparison of the linear and nonlinear responses provides useful information for the real implementations and flight test. In addition, both of the systems show similar behaviors in the hovering scenario. To navigate the systems in $X-Y$ plane, LQR-Servo type of control systems is designed as the X and Y positions are defined as the outputs. Figure 4.3 shows that the reference tracking performances are similar for both of the systems. In addition, the linear and nonlinear responses are almost identical. As seen in the plot of θ_1 vs. time, the attitude dynamics of the basic and advanced systems are similar, as well. The nonlinear responses have slightly higher overshoots compared to that of the linear ones at the beginning. However, the basic and advanced systems unveil dissimilar orientations, θ_2, of limb *BD*. Distal limbs show unlike responses as two systems are compared. It is seen that the limb DG presents quite unlike behaviors after 10^{th} second during the motion along the X axis and landing down. As seen in Figure 4.4, the utilized control inputs show differences for the linear and nonlinear responses in the transient region especially. This must be noted for the real experiments.

The disturbance rejection ability of the flying systems is a necessity in real operations. In order to test the relevant performances, the external forces in Figure 4.5 are acted at the tip point of the distal limbs. Figure 4.6 shows that the control system revealed a robust performance in tracking the reference positions for X and Y axes. In terms of

the attitude response, θ_1, the linear responses of basic and advanced systems are reasonably similar. However, nonlinear responses present high amplitude variations. The limbs *BD* expose diverse responses in terms of θ_2. The linear and nonlinear responses, θ_2, for the basic system are extremely different. Whereas those for advanced system are reasonably similar to each other. The distal limb for the advanced system present dissimilar linear and nonlinear responses. It is concluded that the proximal limbs of the basic and advanced systems reveal similar responses. For both of the systems, the reference input tracking performance is robust due to the applied external disturbances in both linear and nonlinear responses. Table 2 shows that the basic system has a better tracking performance in Y axis and the advanced system has a superior performance in X axis. Considering the real implementations, the nonlinear responses show differences as they are compared with the linear ones. However, the applied control system imposes a strategy to track the given position references. Figure 4.7 shows the utilized control inputs with differences for linear and nonlinear responses. However, they are still feasible considering the possible physical actuators.

The behaviors of the systems are assessed as the compelling types of external forces in Figure 4.8 are applied to the systems. The control systems and gains are the same for navigation control, navigation control with external forcing and the navigation control as the compelling external forces are applied. In the Figure 4.9, the linear response of the basic system presents that the external disturbances are rejected. However, the nonlinear response of the basic system diverges. This difference may break down the physical system as we only rely on the linear response. The same external forces are applied on the advanced system and in Figure 4.10 it is shown that the system has the potential to reject the disturbances. Both the linear and nonlinear responses show quite similar behaviors. Instead of *rejecting* the effects of the external forces, *interacting* with them changes the behavior of the basic system. The admittance control system reshapes the reference inputs for X and Y positions to be tracked by the system. The introduced compliance enhanced the relative stability of the nonlinear system.

CHAPTER 6

CONCLUSION

In this thesis, class of a robotic system with the multi-modal locomotion ability is introduced. The basic and advanced forms are discussed. In air motion of the systems are modeled in 2D space. Due to the inherent instability of the systems, a control system is required to maintain the hovering and navigation performance. Linear-quadratic-regulator based control systems are designed and implemented on the linear and nonlinear systems. This topology is a popular and typical one that is widely used for flying robots [14-17]. The analysis on the basis of the employed control topology shows that the advanced system has superior disturbance rejection capacity. The proximal limbs unveil similar responses. The comparisons reveal that it is feasible to lock the joint at *D* and use the advanced system reducing to the basic configuration to minimize the utilized energy in case of naïve disturbances. Combined with the admittance controller the systems are suitable to be used as aerial manipulators. The second stage of the study will focus on the physical implementation. Indoor localization will be performed based on the Ultra Wide Band (UWB) localizationsystem as experienced in [18].

CHAPTER 7

FUTURE WORK

The physical tests and implementations are left as future work to be completed in another thesis study. Derive mathematical models, control systems, and the simulations will guide the upcoming study. The ground locomotion is out of scope of the thesis. It will be covered in other theses studies. As a notice, the basic and advanced systems will have different natures of ground locomotion due the difference in the number of joints.

The designed controllers will be easily implemented in real-time by the flight control systems such as Pix hawk, Naze 32, etc. In indoor tests, the position of the center of mass will be sensed by the Ultra Wide Band Localization system. The angular velocities of the chassis and the limbs will be obtained by the aid of inertial measurement unit and the utilized gyros on the limbs. In this thesis, it is assumed that the external forces acting on the tip point of the distal limb are measured by the aid of the force transducers at the tip. Typical transducers are available in the market. In addition, estimators can be designed to estimate the external forces.

The prototypes are suitable to be used in multi-modal locomotion research. In addition, they can be utilized as aerial manipulators. Their physical structures make them to be utilized in a collaborative transportation system, as well.

REFERENCES

[1] L. Daler, S. Mintchev, C. Stefanini, D. Floreano. A bio inspired multi-modal flying and walking robot. Bio inspir. Biomim. 10 (2015) 016005

[2] C. Premachandra et al. A study on development of a hybrid aerial/terrestrial robot system for avoiding ground obstacles by flight. IEEE/CAA Journal of Automatica Sinica, 2018. **6**(1): pp. 327-336.

[3] N. Meiri and D. Zarrouk. Flying star, a hybrid crawling and flying sprawl tuned robot in 2019 International Conference on Robotics and Automation (ICRA). 2019. IEEE

[4] Y. Yu and X. Ding. On hybrid modeling and control of a multi-propeller multifunction aerial robot with flying-walking locomotion. Autonomous Robots, 2015. **38**(3): pp. 225-242.

[5] S. Mintchev and D. Floreano. A multi-modal hovering and terrestrial robot with adaptive morphology. in Proceedings of the 2nd International Symposium on Aerial Robotics. 2018.

[6] P. Ratsamee et al. A hybrid flying and walking robot for steel bridge inspection. In 2016 IEEE International Symposium on Safety, Security, and Rescue Robotics (SSRR). 2016. IEEE.

[7] S. Latscha et al. Design of a Hybrid Exploration Robot for Air and Land Deployment (HERALD) for urban search and rescue applications. in 2014 IEEE/RSJ International Conference on Intelligent Robots and Systems. 2014. IEEE.

[8] D. Wei et al. Hybrid Inspired Research on the Flying-Jumping Locomotion of Locusts Using Robot Counterpart. Frontiers in neurorobotics, 2019. **13**: p. 87.

[9] J. Zhao et al. Controlling aerial maneuvering of a miniature jumping robot using its tail. in 2013 IEEE/RSJ International Conference on Intelligent Robots and Systems. 2013. IEEE.

[10] D. Küçük. Design of Two Wheeled Twin Rotored Hybrid Robotic Platform, MSc. Thesis, Department of Mechatronics Engineering, Atılım University, 2010.

[11] C.J. Pratt and K.K. Leang. Dynamic underactuated flying-walking (DUCK) robot. In 2016 IEEE International Conference on Robotics and Automation (ICRA). 2016. IEEE.

[12] Nik L.M. Grubben & Karel J. Keesman (2018). Controllability and observability of 2D thermal flow in bulk storage facilities using sensitivity fields, International Journal of Control, 91:7, 1554-1566.

[13] A. Taglibue, M. Kamel, S. Verling, R. Siegwart, J. Nieto. Collaborative Transportation Using MAVs via Passive Force Control, IEEE International Conference on Robotics and Automation (ICRA), 2017.

[14] Y. Zhi, G. Li, Q. Song, K. Yu & J. Zhang (2017). Flight control law of unmanned aerial vehicles based on robust servo linear quadratic regulator and Kalman filtering. International Journal of Advanced Robotic Systems.

[15] L. Martins, C. Cardira, P. Oliveira. Linear Quadratic Regulator for Trajectory Tracking of a Quadrotor, IFAC Papers Online 52-12 (2019) 176–181.

[16] Xie Heng, David Cabecinhas, Rita Cunha, Carlos Silvestre and Xu Qingsong (2015). A Trajectory Tracking LQR Controller for a Quadrotor: Design and Experimental Evaluation, TENCON 2015 - 2015 IEEE Region 10 Conference.

[17] Q. Ali, S. Montenegro (2016). Decentralized Control for Scalable Quadcopter Formations, International Journal of Aerospace Engineering.

[18] A.T. Başaranoğlu (2019). Design of Control Systems for an Aerial Manipulator. MSc. Thesis, Department of Mechatronics Engineering, Atılım University.